



DEPARTMENT OF INFORMATICS

TECHNISCHE UNIVERSITÄT MÜNCHEN

Bachelor's Thesis in Informatics

LiDAR and Camera Data Fusion for the Biologically Inspired SLAM Systems

LiDAR und Kameradaten Fusion für die Biologisch Inspirierten SLAM-Systeme

Author: Jakub Šťastný
Supervisor: Prof. Dr.-Ing. habil. Alois C. Knoll
Advisor: Genghang Zhuang, M.Eng.
Submission Date: 15.09.2022



I confirm that this bachelor's thesis in informatics is my own work and I have documented all sources and material used.

Munich, 15.09.2022

Jakub Šťastný

Abstract

Simultaneous localization and mapping is a crucial problem for most autonomous mobile robots. RatSLAM is a biologically inspired SLAM system that simulates the rodent's brain using the Pose Cell network, odometry, and visual input. This system demonstrates long-term stability and accurate results in indoor and outdoor environments. One of the essential parts of RatSLAM is a scene recognition algorithm. Whereas RatSLAM uses a visual scene recognition approach, this work suggests a technique to combine data from 3D LiDAR and camera to achieve better scene recognition results and hence improve the whole SLAM system. Compared to the camera, the LiDAR sensor is more accurate and robust to changing light conditions. This thesis proposes several scene recognition approaches using combined data from the camera and 3D LiDAR sensor. These approaches are combined with RatSLAM to build an improved biologically inspired SLAM system. All proposed methods are tested on performance using several evaluation metrics and compared with visual scene recognition and OpenRatSLAM. As the results show, the suggested methods are capable of accurate and robust scene recognition, and final SLAM systems are able to construct suitable experience maps. Furthermore, all proposed approaches outperformed the OpenRatSLAM in most of the evaluated metrics and worked smoothly also in situations where OpenRatSLAM failed.

Kurzfassung

Simultaneous localization and mapping ist ein entscheidendes Problem für die meisten autonomen mobilen Roboter. RatSLAM ist ein biologisch inspiriertes SLAM-System, das das Gehirn des Nagetiers mithilfe des Pose Cell-Netzwerks, Odometrie und visueller Eingabe simuliert. Dieses System zeigt langfristige Stabilität und genaue Ergebnisse in Innen- und Außenumgebungen. Einer der wesentlichen Bestandteile von RatSLAM ist ein Szenenerkennungsalgorithmus. Während RatSLAM einen visuellen Szenenerkennungsansatz verwendet, schlägt diese Arbeit eine Technik vor, um Daten von 3D-LiDAR und Kamera zu kombinieren, um bessere Ergebnisse bei der Szenenerkennung zu erzielen und somit das gesamte SLAM-System zu verbessern. Im Vergleich zur Kamera ist der LiDAR-Sensor genauer und robuster gegenüber wechselnden Lichtverhältnissen. Diese Arbeit schlägt mehrere Ansätze zur Szenenerkennung vor, die kombinierte Daten von der Kamera und dem 3D-LiDAR-Sensor verwenden. Diese Ansätze werden mit RatSLAM kombiniert, um ein verbessertes biologisch inspiriertes SLAM-System aufzubauen. Alle vorgeschlagenen Methoden werden anhand mehrerer Bewertungsmaßnahmen auf ihre Leistung getestet und mit visueller Szenenerkennung und OpenRatSLAM verglichen. Wie die Ergebnisse zeigen, sind die vorgeschlagenen Verfahren zu einer genauen und robusten Szenenerkennung in der Lage, und endgültige SLAM-Systeme sind in der Lage, geeignete Erfahrungskarten zu erstellen. Darüber hinaus übertrafen alle vorgeschlagenen Ansätze OpenRatSLAM in den meisten der bewerteten Metriken und funktionierten reibungslos auch in Situationen, in denen OpenRatSLAM versagt hat.

Contents

Abstract	v
Kurzfassung	vii
1 Introduction	1
1.1 Motivation	3
1.2 Objectives	3
1.3 Work Contribution	4
1.4 Outline	5
2 Related Work	7
2.1 Scene Recognition Problem	7
2.1.1 Local Image Descriptors	7
2.1.2 Global Image Descriptors	8
2.1.3 Neural Networks Based Approaches	8
2.2 OpenRatSLAM	9
2.2.1 Local View Match	9
2.2.2 Visual Odometry	9
2.2.3 Pose Cell Network	10
2.2.4 Experience Map	11
3 Technical Background	13
3.1 Robot Operating System	13
3.2 Gazebo	15
3.3 Turtlebot3	15
3.4 RViz	15
3.5 OpenCV	16
3.6 Pytorch	16
3.7 PointNet	16
3.8 Color Models	16
4 Methodology	19
4.1 Problem Definition	19
4.2 System Architecture	20
4.2.1 Robot Simulator	20
4.2.2 Data Fusion	21
4.2.3 LV Builder	21

4.2.4	LV Matching	21
4.2.5	Rat SLAM ROS	22
4.2.6	LV Analyzer	23
4.2.7	LV Dataset Creator	23
4.3	Data Fusion and Preprocessing	24
4.3.1	Sensors Synchronization	24
4.3.2	Data Fusion	26
4.3.3	Ground Removal	27
4.4	General Scene Recognition Outline	28
4.5	Hierarchical View Matching Based on Clustering	28
4.5.1	Template Extraction	30
4.5.2	Template Matching	31
4.5.3	Automatic Parameter Tuning	33
4.6	Neural Networks Based View Matching	34
4.6.1	Networks Structure	35
4.6.2	Training of the Networks	35
4.7	2-stage View Matching	35
4.7.1	Template Building	36
4.7.2	Template Matching	36
5	Experiments	37
5.1	Used Environments	37
5.2	Evaluation	39
5.3	System Setup	40
5.4	Accuracy	41
5.5	Average False Positive Error	44
5.6	Time Performance	46
5.7	Memory Consumption	50
5.8	RatSLAM Integration	51
5.9	Discussion	51
6	Conclusion and Future Work	57
6.1	Limitations	57
6.2	Future Work	58
List of Figures		59
List of Tables		61
Bibliography		63

1 Introduction

Nowadays, mobile robots are becoming more and more popular. Whether it is an autonomous car, a transport robot in a warehouse, or an automatic vacuum cleaner, these robots are finding more and more applications and becoming a part of most people's everyday lives.

One of the essential tasks every mobile robot must be able to solve is finding a valid path from its current position to the target based on the obstacles and surroundings. Knowledge of the robot's precise location and environment map is a necessary prerequisite for almost any navigation and planning algorithm.

Even if most of the world is already mapped on a large scale and due to GPS, Gallileo, GNSS, etc., we can locate ourselves on these maps with satisfiable accuracy, these methods can not be usually used for the indoors or small scale environments, where the maps are typically unknown, and any global positioning services can not be used.

Furthermore, a proper self-localization of the robot depends on a precise map, and map construction depends on the accurate positions of a robot and other landmarks. Therefore the localization and mapping problems have to be usually solved simultaneously. In addition, the environment can frequently change, which makes, together with the mutual dependence of localization and mapping, the simultaneous localization and mapping (SLAM) a very challenging problem, that most mobile robots must solve.

The SLAM has been solved by many scientists since the 1980s. Until now, there have been developed many different techniques for solving the SLAM, with various advantages and disadvantages. The majority of the approaches can be separated into three main categories: conventional SLAM, visual SLAM, and biologically inspired SLAM.

The conventional algorithms are based on a probabilistic model and usually work with Light Detection And Ranging [1] and odometry sensors. These techniques typically work in two steps. In the first step, the position of the robot and landmarks are extracted from the raw sensor data, usually using different filtering techniques, such as Kalman filter or particle filtering. This extracted information is used in the second step to build or update the final map.[2]

The precision and resolution of the final maps built by these approaches are usually very high. However, there is usually a high computation and storage demand that rapidly increases with the number of landmarks. Because of this fact, the conventional techniques are generally not suitable for larger or complicated environments with a lot of landmarks and can not be performed on low-performance computation devices, such as older Raspberry PI models. Furthermore, many of these techniques usually rely on accurate sensor measurements and are not robust against more significant measurement

errors that can easily destroy the whole map.

The visual SLAM approaches became popular mostly during the last decade, with cameras' significant cost reduction and quality improvement. As the name suggests, these techniques are based on visual input from a 2D or 3D camera and various computer vision techniques. Compared to conventional methods, these approaches obtain more information about the environment and, therefore, can generate more precise outputs. However, most visual SLAM methods are susceptible to ambient lighting and reflections and perform differently in different light conditions, which can cause significant errors. Furthermore, these techniques work poorly in a low-texture environment, making them unsuitable for environments with many windows, mirrors, or other glass or reflective surfaces.[3]

As the name suggests, the biologically inspired SLAM approaches find their inspiration in various biological systems. The ideas behind these techniques are very diverse and differ from approach to approach. In this category, we include techniques based on machine learning, models of biological structures, or methods based on the behavior of some biological species. These techniques usually can not guarantee the result's precision but use a heuristic approach to approximate the results with specified accuracies. These techniques generally have a significantly lower demand for resources than conventional and visual approaches. Furthermore, these techniques are usually more robust against measurement errors and can also contain a mechanism to repair the previous errors based on the new data.

One of the most generally known biologically inspired SLAM systems is RatSLAM, which was initially developed in 2008 and improved over the years [4]. The open source version of this technique, the OpenRatSLAM [5], and its ROS implementation RatSLAMRos [6] brings a standardized, reconfigurable, and modulized way to include this method to any program for mobile robots. Furthermore, the RatSLAM approach shows long-term stability in the indoors and outdoors scenarios.[7][8][9][10]

This approach is inspired by computational models of the hippocampus of rodents, which have been extensively studied concerning navigation tasks and show many of the properties of a desirable SLAM solution. During the last 50 years, four essential kinds of neurons have been discovered connected with SLAM and navigation tasks: place cells, grid cells, head direction cells, and border cells.

Place cells, discovered by John O'Keefe in 1976 [11], are connected with different places the rodent has visited and are activated every time the rat returns to a particular location. Grid cells, discovered by Edvard and May-Britt Moser in 2008 [12], react to the rodent's movement and are activated in sequence as the rat moves around in the environment. The head direction cells allow the rodent to get the spatial sense of direction based on geometry features. Finally, the border cells are activated when the rodent moves close to a wall or other obstacle.

According to biological inspiration, localization is based on odometry, inspired by the Grid cells. Odometry is well known for its problems with cumulative errors. It does not matter how precise odometry sensors or techniques are used; even a very small error

adds up over time, and the whole system will be completely out of reality after a few minutes, maximally a few hours. To reduce these errors, a loop closure technique is required. Based on the biological model, the RatSLAM implements the loop closure using a place recognition technique.

So, place recognition is one of the crucial parts of the RatSLAM solution and any intelligent system operating autonomously over a longer period of time. The main task of this problem is to tell if the robot has visited the current place before or not, despite several changes in its appearance due to different light conditions, weather, or non-stationary objects like pedestrians or cars.

Most standard place recognition techniques are based on visual input and usually use machine learning, feature extraction and matching, or the scene decomposition approaches. However, some other methods exist based on entirely different ideas and kinds of sensors.

1.1 Motivation

The original RatSLAM approach uses a low-resolution camera image as an input for place recognition. However, as mentioned before, this brings some drawbacks, like sensitivity to the different light conditions and reflections. Compared to a camera, a 3D LiDAR sensor can measure directly in three dimensions with a high precision, even over a long distance. Furthermore, the 3D-LiDAR sensor is robust against different light conditions and reflections. On the other hand, compared to the camera, the LiDAR data lose some helpful information, like colors, that can be a critical factor in place recognition of places in the environments like office buildings with different meeting rooms that differ only in the wall color and otherwise remain identical.

The proper combination of the advantages of both these sensors can significantly improve place recognition and consequently enhance the quality of the entire RatSLAM algorithm. Furthermore, the additional odometry sensor may provide more accurate speed data, improving the SLAM quality compared to the original RatSLAM, which calculates odometry information only from the visual input.

Lastly, place recognition based on visual data requires storing whole images or extracted feature vectors, which consumes a relatively large amount of memory. The proper representation of the scene based on the LiDAR and camera data may significantly improve the required space and make RatSLAM even more suitable for the low performant computational devices.

1.2 Objectives

This thesis aims to find an optimal method of combining data from several sensors and find the best solution for the place recognition problem and, as a result, improve the precision and performance of the RatSLAM algorithm. Besides, all suggested approaches find inspiration in biological systems, like the rest of the RatSLAM approach.

To achieve this primary goal, several challenges need to be solved. The first challenge is data fusion. In this part, the optimal scene representation must be designed to combine most of the information from all the sensors and reduce most of the disturbing factors typical for the input sensors. Furthermore, the synchronization and mutual calibration of the sensor must be solved.

The other challenge is to solve the place recognition problem based on the representation from the fused data. In this part, we need to think apart from accuracy to the performance and memory consumption in order to make this approach available for low-performance devices.

There will be suggested several algorithms with different expected advantages and disadvantages. All proposed techniques will be tested on accuracy and various performance metrics and compared to each other, as well as to an image-based place recognition used in an original RatSLAM.

1.3 Work Contribution

First, I came up with a compact scene representation that combines the advantages of both LiDAR and the camera. Then I suggested a practical approach to fuse the data received from the sensors into the chosen representation. This part also contained sensor synchronization and calibration.

Afterward, I designed a compact and suitable scene template that will be stored in the memory. While creating the template, I followed the biological inspiration, namely the model of human spatial memory. I also devised a method to extract the designed template from the fused scene representation effectively. Finally, after preparing the template model, I created an approach to compare two of these templates and thus solved the scene recognition problem.

The suggested algorithm was based on scene decomposition, object detection, and extraction of the significant properties of each object. However, this approach did not consider the objects' exact shape, leading to a considerable increase of false positive evaluations in several environments. To eliminate these false positive evaluations, I came up with a 2 stage approach. This approach was based on the originally designed method. All scenes were evaluated same as before; however, all positive evaluations were re-evaluated using a neural network in the second stage.

To create a working second stage, I choose suitable network architecture and experimentally found the best network's dimensions. After deciding on the network architecture, I made appropriate training datasets and trained and tested the model.

The suggested approach was dependent on many different parameters. The optimal parameters had to be found to maximize the place recognition performance. So, I came up with an optimization method that finds an optimal parameters vector, maximizing the approach's accuracy. In order to implement this optimization method, I created a set of tools for manual and automatic performance testing and analysis.

After the scene recognition algorithm was finished, I successfully integrated it with

RatSLAM and created a robust biologically inspired SLAM system. I made the whole system in ROS to ensure its modularity, reconfigurability, reusability, and easy improvement.

After creating the whole system, I devised several evaluation metrics to test all critical methods' properties. I set up a robust testing simulation in several environments and created reusable testing datasets to ensure the reproducibility of all experiments. Finally, I tested all suggested techniques and the OpenRatSLAM approach, found an appropriate presentation of the results, and compared all presented methods.

1.4 Outline

Chapter 2 presents a related work about various scene recognition approaches and biologically inspired SLAM systems.

Chapter 3 describes all frameworks and tools used in this work.

Chapter 4 provides a detailed description of all the algorithms and techniques implemented in this thesis. Namely, the complete system overview is provided in the beginning, followed by the solution to the data fusion problem. Afterward, three different place recognition techniques are offered.

Chapter 5 evaluates the performance of approaches presented in chapter 4 and compares them with the OpenRatSLAM. The beginning of the chapter introduces the test environments and evaluation metrics. The following four sections will discuss the results of the different evaluation metrics. In the penultimate section will be tested the integration of the place recognition approaches with RatSLAM. Finally, the last section summarizes all measured results and discusses all suggested techniques' final performance and advantages or disadvantages.

Chapter 6 summarizes the whole work, alerts to possible drawbacks, and suggests future work.

2 Related Work

2.1 Scene Recognition Problem

Scene recognition is a problem that received a lot of attention from many researchers and engineers in the last few years. Even if approaches for several sensors were developed, the most popular is visual scene recognition based on images from a camera.

This section presents some of the most popular approaches for visual scene recognition based on traditional methods and machine learning.

2.1.1 Local Image Descriptors

This technique aims to find, describe and compare significant features from the images. Each image is processed in two phases: detection and description. Since both stages can be solved independently, a large number of various approaches for each phase have been developed.

The detection phase aims to detect all essential features in a given image, such as edges, corners, significant points, or objects. The feature detection algorithms generate pixel coordinates of each feature, usually with an occupied area. An example of the detected features in an image is shown in Figure 2.1. There are many different approaches to this problem, like FAST [13], Laplacian of Gaussian [14], SUSAN [15], and many more, detecting different kinds of features.



Figure 2.1: Example of detected features in the image. [16]

The goal of the description phase is to provide a summary of the image information around each feature. The feature is represented as its position in the image, and the

output is defined as an N-dimensional vector. A good feature descriptor should fulfill three following rules: Repeatability, Distinctiveness, and Efficiency. The repeatability means that the feature descriptor is robust and invariant to the image's translation, rotation, or illumination changes. Distinctiveness represents the ability to distinguish between two close features. Finally, due to real-time processing, which is increasingly applied nowadays, efficiency also plays an important role. Among popular approaches to solve this problem can be included SURF [17], GLOH [18], BRIEF [19], and many more.

Using these two stages, the set of local image descriptors

$$\mathbf{X} = [\mathbf{x}_0, \mathbf{x}_1, \dots, \mathbf{x}_{n-1}]^T$$

is extracted, in which $\mathbf{x}_i \in \mathbb{R}^k$. However, each image can contain hundreds of individual features, which can be impractical in real-time processing and requires a huge amount of memory. To lower the dimensions of the local descriptors vector, different techniques like bag-of-visual-words [20][21], VLAD [22], or Fisher kernel [23] may be applied to aggregate the vector \mathbf{X} into a more compact single vector. Finally, these vectors are compared to decide if two images represent the same place. The precise comparison technique depends on the techniques used in the description phase and for the final descriptors' vector compression.

2.1.2 Global Image Descriptors

This technique works similarly to the previous one, with one big difference. In this approach, the detection phase is wholly omitted, and the whole image is considered as only one feature. Therefore, the feature description algorithms must be modified to suitably describe large and diverse features. Some alternations of the algorithms provided in the last part might be WI_SURF [24] or BRIEF-GIST [25].

2.1.3 Neural Networks Based Approaches

Convolutional neural networks achieve outstanding performance on several recognition or classification tasks, including a solution to scene recognition problems [26] [27]. The basic idea behind this approach is similar to the previously presented technique. In the first step, the global feature descriptor is extracted from the image and afterward compared with the other extracted feature vectors. However, unlike the previously presented technique, this approach uses machine learning instead of classical techniques to perform these two tasks.

According to the studies [28][29], the features extracted from images using convolutional neural networks significantly outperform the features extracted by classical algorithms like SIFT. There are many different kinds of convolutional neural networks used for these purposes. From the most popular ones, we can mention VGGNet [30] or GoogleNet [31].

2.2 OpenRatSLAM

OpenRatSLAM is an open source version of the RatSLAM approach implemented in ROS, see section 3.1. The system consists of the three most crucial components: Local view match, pose cell network, and experience map. Furthermore, the system contains one additional node, visual odometry, that can be optionally used to replace the odometry sensor with visual input. The way how these four parts communicate is presented in the picture 2.2.

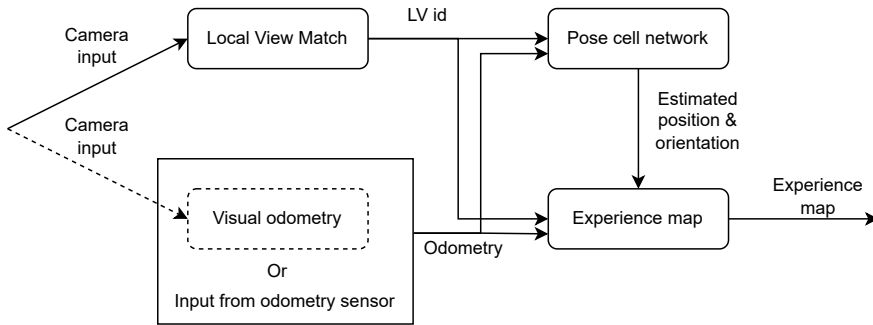


Figure 2.2: Nodes communication structure in the OpenRatSLAM

This section briefly introduces how each part of the RatSLAM works. For the detailed description, see [4] [5].

2.2.1 Local View Match

This node receives an image from the camera and returns the id of the matched scene or a new id if no match is found. Firstly, the received image is converted into a local view template, represented as a strongly compressed grayscale image¹. Before the conversion, global and local normalization steps are performed to lower light condition errors. After the normalization, the image is suitably compressed and converted to a grayscale image.

The generated template is compared with all the previously stored templates by calculating the sum of absolute differences. If the best result is below the chosen threshold, the id of the most similar scene is returned. If the best result is above the threshold, the scenes are estimated as different, and the current view template is stored with a new id, which will be returned.

2.2.2 Visual Odometry

This node's usage is necessary only when there is no odometry input from the sensors. This node aims to generate odometry data from camera input and thus replace the odometry sensor. The translational and rotational speed is calculated from changes in two regions of interest chosen in the incoming images. See [8] for more details.

¹In the experiments were used images with 60x10 px

2.2.3 Pose Cell Network

A pose cell network is a 3D structure of cells structured in a grid. Every cell represents a combination of the robot's position on x and y axes and orientation on the z axis. The grid is also cyclic, meaning that the right-most cells are neighbors with the left-most cells or that the cells at the bottom are neighbors of the cells at the top of the grid. Each cell has an activity level, expressed by a real number between 0 and 1, where one means high activity and zero means no activity. Together with the grid of the pose cells, there exists a set of local view cells. The cells in this set arise during the program run, and every local view cell is connected with precisely one pose cell in the grid network. The network is visualized in Figure 2.3

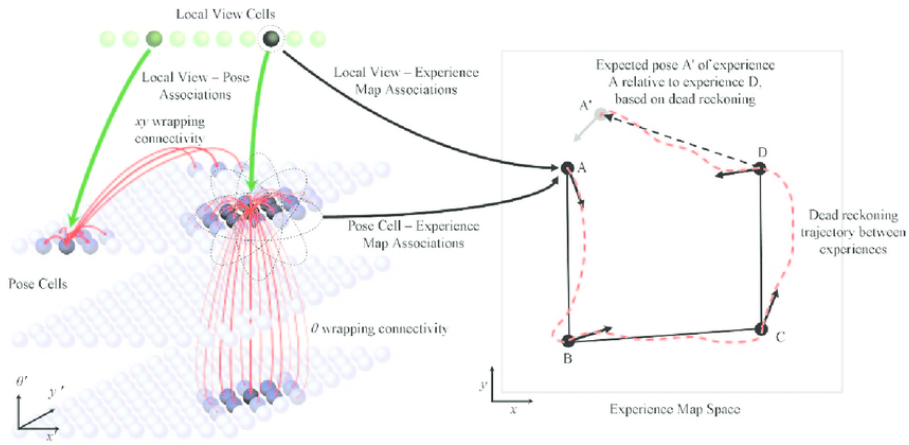


Figure 2.3: The OpenRatSLAM system structure. [9]

During the algorithm run, there are usually more active pose cells. The bunch of active neighboring cells is called an activity packet. The final pose of the robot is estimated as the centroid of the activity packet. In the ideal situation, the grid contains only a single activity packet. However, several distinct activity packets could arise due to errors or inaccuracies in the sensors' data or LV match. In this case, the final pose is calculated as a centroid of the packet with the highest activity level.

Every time the Local view match node publishes an entirely new LV id, a new LV cell is created, connected with the pose cell representing the estimated current robot's position, and activated. When a known id is published, the corresponding local view cell is activated. There is always exactly one active local view cell.

The network's activity is updated in several steps: visual association, path integration, and normalization. At the beginning of the update step, the activity level of the cells around the pose cell, connected with the activated local view cell, is excited or inhibited according to the normal distribution. The path integration process projects the activity of the pose cells into cells near the currently activated ones. If the robot is translating, the activity is shifted in the xy plane; if the robot is rotating activity is shifted in the z direction. Under translation, the direction of movement of activity is dependent upon

the cell's position in the z direction. The magnitude of the movement in the xy plane and z axis depends on the translational and rotational velocity.[4] The total activation level of the network is designed to be 1. Therefore, after performing the visual association and path integration phases, the activity level of all the cells is normalized.

2.2.4 Experience Map

The experience map produces a graph-like map based on the network's activity, which is the final output of the algorithm. The map nodes, called experiences, correspond to the individual positions estimated by the pose cells together with the estimated local views. The experiences are connected with the links containing information about the relative pose, estimated from the odometry data and updated over time.

The map contains a map relaxation technique, which merges or removes experiences based on their similarities and accumulated errors. This technique makes the map more compact and the whole algorithm more robust against measures or estimation errors.

3 Technical Background

This chapter provides an overview of most of the techniques, frameworks, and libraries related to the thesis, including the Robot Operating System ROS, Gazebo, Turtlebot3 models, RViz, OpenCV, Pytorch, PointNet, and different models used for the representation of colors and calculating of their differences.

3.1 Robot Operating System

Robot Operating System[32], shortly ROS is a popular open-source framework commonly used by many researchers and robot developers. This framework allows easy launch, deployment, and communication between different modules as standalone services that create a final complex system. This modularity permitted the creation and easy application of various tools and libraries like Gazebo, RViz, or rqt, together with custom services. Furthermore, the ROS allows an easy spread of one system among more devices, allowing an easy run of some services directly on the robot and other services on the central computer, without almost any accessive work.

Another significant advantage of the ROS's modularity is that you can exchange the robot simulator with the real robot and sensors without touching the rest of the system. Furthermore, you can record and replay the entire system's messages during its run, allowing easy reproducibility of any experiment.

The official languages of the ROS are C++ and Python, but there are also unofficial tools that allow writing services for ROS in other languages, like, for example, LISP [33] or Swift[34].

The following subsections briefly introduce some of the essential ROS features.

Roscore

Roscore is a service that must be executed before running any Node of the ROS system. This service will automatically start all the essential services for the ROS running, like logging service, parameter server, and ROS master. Therefore, the running roscore service is necessary for ROS nodes to communicate.

ROS Node

Ros Nodes are a crucial concept of the whole system. Single Node represents a standalone service that can process data received from other ROS Nodes, sensors, or users and send them to the other Nodes or directly to the user or system actors. The entire

application usually consists of many ROS Nodes that communicate using ROS topics, services, etc.

ROS Message

Messages are the most common way of communication between several ROS Nodes. These messages are transmitted between the Nods via ROS topics. The ROS message, typically stored in the .msg file, describes a format that the data transmitted on a particular ROS topic must fulfill and tells the ROS Node how to represent the received data.

According to the convention, most messages start with the Header part, containing the message sequence number, timestamp, and frame id. However, this header is optional and is not present in some commonly used messages.

ROS Topic

ROS topics are named buses, serving for message exchange between the Nodes. One or more nodes can publish messages or subscribe to each ROS topic and receive all published messages. The publishing and subscribing processes work anonymously, which means that the publisher does not know if the message was read by only one or more or any node, and receivers do not know which node published the particular message unless it's part of the sent data.

Every topic is strongly connected with a particular message type, so every message published on the same topic must have the same format.

Roslaunch

Roslaunch is a tool allowing the launch of multiple ROS Nodes with a single command based on an XML configuration. This tool also supports setting different parameters that can be set while starting the process and passed to the particular Nodes or put on the Parameter Server. Furthermore, this tool allows renaming specified topics without the need to tell any information to the publishing Nodes.

ROS package

ROS packages help to organize the ROS software. The package can contain ROS Nodes, libraries, datasets, configuration files, etc. The goal of the ROS package is to pack together connected ROS Nodes and other tools that together create some meaningful tool, program, or library. These packages allow easy publication, deployment, installation, and integration of the third-party components into custom programs or systems.

Rosbag

Rosbag is a command line tool for recording and replaying the data exchanged between Nodes during the program run. This tool can record all messages published on all or only specified ROS topics without affecting the running system. These messages can be later replayed, which allows excellent reproducibility of all program runs and further optimization, improvement, and testing under the same conditions.

Particularly researchers with this tool record all data from the sensors while running experiments and publish them on the internet for later experiment reproduction or further development.

Catkin

Catkin is a collection of CMake macros and Python scripts commonly used for the ROS development and building of ROS Nodes and packages. Even if catkin is not the official part of ROS, it is a widely used tool among the ROS community.

3.2 Gazebo

Gazebo is a famous open-source 3D-simulation tool supporting robot simulation in complex 3D environments, including realistic physics, like gravity, friction, collisions, light reflections, etc. These environments can also change over time, which allows adding pedestrians, moving cars, or other non-stationary objects to the simulation.

Furthermore, Gazebo supports various types of sensors, especially HD-Camera, 3D or 2D LiDAR, IMU, etc., or several plugins for the robot control. This tool also provides an interface fully compatible with ROS, which makes it a perfect simulation tool for this thesis.

3.3 Turtlebot3

Turtlebot3 offers open-source mobile robots commonly used in robotics research and development. The Turtlebot3 provides two different models, Burger and Waffle-Pi, that are fully compatible with the Gazebo simulator and contain all software necessary for the robot control and simulation. These models are also easily extensible and allow adding new kinds of sensors.

3.4 RViz

RViz is a ROS graphical interface, allowing the visualization of the information published for many different available topics. Particularly, this tool is commonly used for the real-time visualization of the data received from various sensors, generated maps, landmarks, detected objects, etc.

3.5 OpenCV

OpenCV[35] is an open-source computer vision library available for C++ and Python. This library contains many real-time image and video processing tools, from simple transformations to feature extraction and matching or object recognition.

3.6 Pytorch

Pytorch [36] is a python open-source machine learning framework based on the Torch library. This framework is commonly used in the area of machine learning. It contains many tools for modeling Neural Networks, several training algorithms, tools for datasets preparation, advanced matrix operations tools, etc. Furthermore, because of the CUDA support, this framework allows running most of the calculations on the GPU, which can significantly speed up the training process of most models.

3.7 PointNet

PointNet [37] is a deep neural network widely used for point cloud processing by many applications. This network can extract the feature vector from any point cloud, invariant to the order of the points and the rotation of the scene that the input cloud represents. Furthermore, the input size in terms of the number of points can vary for each input. There is available a C++ implementation [38] of the network, as well as a Python implementation in TensorFlow [39] or PyTorch [40] version.

Except for the feature extraction, the implementations of the PointNet network also include additional networks for scene segmentation and object classification based on the extracted feature vector from the PointNet network. Furthermore, all required learning and dataset preparation algorithms are also included.

3.8 Color Models

There are many different ways to represent a single color on a computer. Except for the well-known RGB representation, there are many different other representations with distinct advantages. Lab [41] representation is for the work the most interesting because it allows easy color difference computation, using CIE76 and CIE2000 formulas [42] that correspond in the best way to the difference told by humans.

Similarly, as in an RGB format, the colors are represented using three different components, L, a, and b. The L part stands for lightness and means how light or dark the color is. The a and b components represent the balance between two different colors. The a part describes the balance between green and magenta, and the b part represents the balance between blue and yellow. Even if this color scheme can describe the whole space of colors, the colors visible by human eyes are located in a sphere, displayed in Figure 3.1.

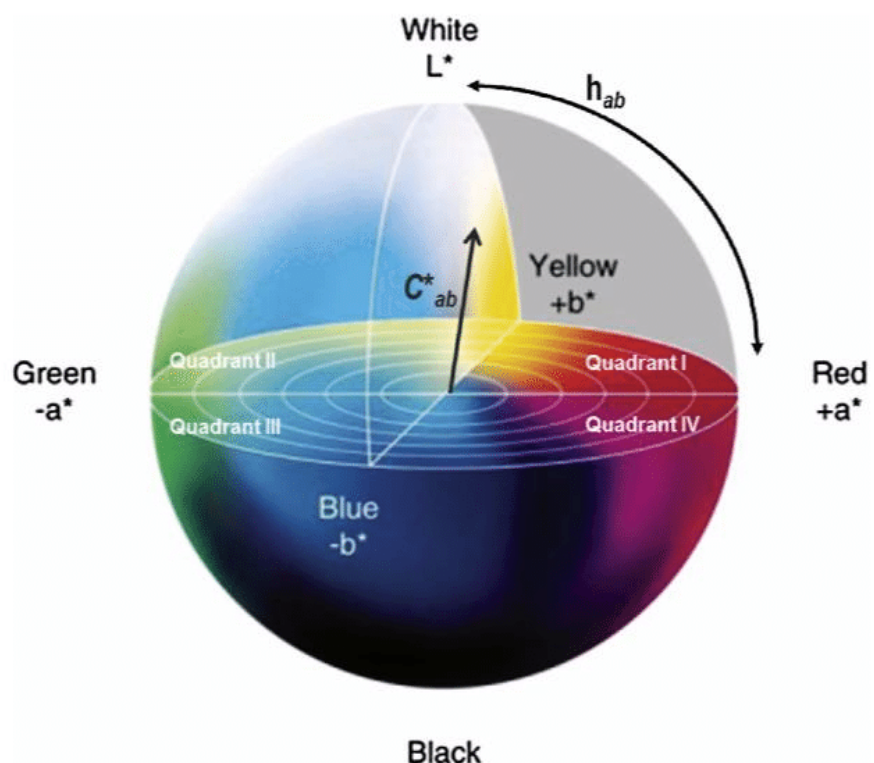


Figure 3.1: Visualization of an Lab color representation [43]

4 Methodology

This chapter provides a detailed description of all the algorithms and techniques implemented in this work. At the beginning of this chapter, the problem is precisely defined. The following section describes a basic system overview with all used components and descriptions

In this thesis, we are mainly solving two problems: data fusion and scene recognition. The approach to solving the data-fusion is described in the third section. The rest of the chapter describes three methods for solving scene recognition problems.

Furthermore, the second section also presents how to connect the data fusion and scene recognition algorithm to the RatSLAM ROS to solve the SLAM problem.

4.1 Problem Definition

1. The scene recognition algorithm receives the data from the unsynchronized sensors, namely the 3D-point cloud from the 3D LiDAR and RGB image from an HD camera. The goal is to recognize if the robot is in the current scene for the first time or if the scene has already been visited. Furthermore, if the scene was already visited, the algorithm must precisely tell which previously visited scene corresponds to the current one. The following steps must be solved:
 - Data synchronization
 - Data fusion
 - Scene recognition
 - **Input:** 3D Point cloud and RGB image
 - **Output:** Id of a corresponding previously visited scene or a new id for the scenes visited for the first time
2. The scene recognition algorithm is integrated with the RatSLAM ROS system to solve the SLAM problem.
 - **Input:** 3D Point cloud, RGB image, odometry
 - **Output:** estimated robot path

4.2 System Architecture

This section presents an overview of the architecture of the whole system. The system is decomposed into several Nodes. Together with the RatSLAM ROS and simulator, the system uses three custom nodes: Data fusion, LV Builder, and LV matching. Furthermore, the system contains two additional nodes that do not influence the algorithm's run but are used for the performance analyses and other help utilities, helping with the development process. The system architecture is presented in Figure 4.1. The visualization and topics used only for visualization purposes are omitted for clarity.

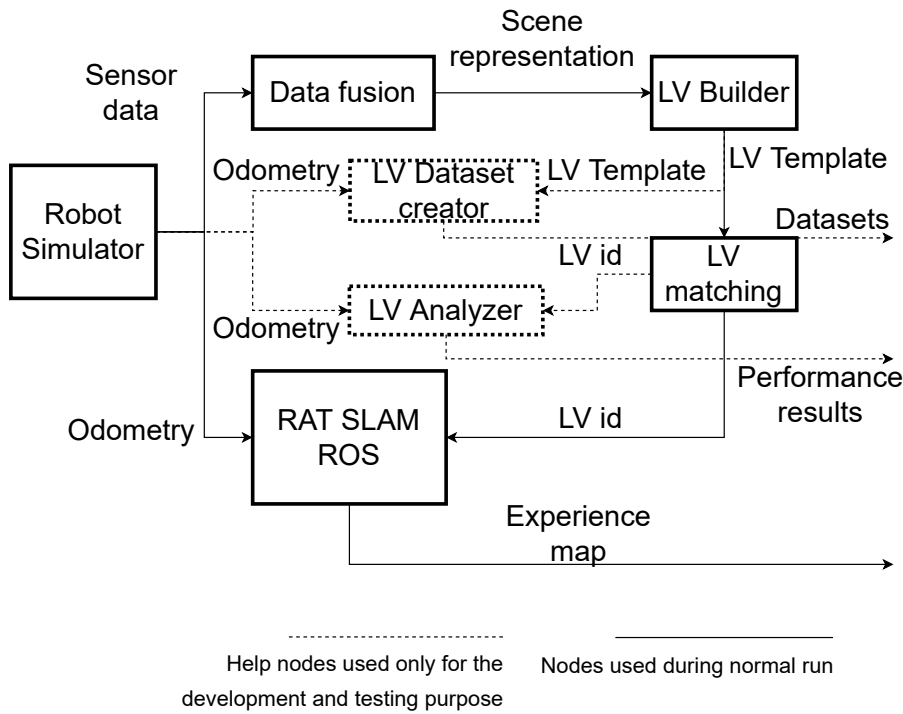


Figure 4.1: Diagram of the ROS nodes in the whole system

4.2.1 Robot Simulator

This node represents the whole simulation and can be easily replaced with a physical robot. The robot is simulated using a Gazebo simulator, introduced in section 3.2. Besides much other information about the scene and the robot, the simulation publishes data from sensors, namely HD Camera and 3D LiDAR, and odometry data, further consumed by other nodes.

Table 4.1: Relevant topics published by the simulator

Topic	Type	Mode
camera/rgb/camera_info	sensor_msgs::CameraInfo	publish
camera/rgb/image_raw	sensor_msgs::CompressedImage	publish
velodyne_points	sensor_msgs::PointCloud2	publish
odom	nav_msgs::Odometry	publish

4.2.2 Data Fusion

The goal of this node is to take raw data from the sensors and create a single representation of the environment, combining the advantages of each sensor. This node takes care of the synchronization of the sensors, dealing with different frames of reference and the fusion itself. The data fusion node subscribes to the camera and LiDAR topics published by simulation or a real robot and publishes one topic with the final environment representation. How this node exactly works is described in the section 4.3.

Table 4.2: Subscribed and published topics by the Data fusion node

Topic	Type	Mode
camera/rgb/camera_info	sensor_msgs::CameraInfo	subscribe
camera/rgb/image_raw	sensor_msgs::CompressedImage	subscribe
velodyne_points	sensor_msgs::PointCloud2	subscribe
rgb_cloud	sensor_msgs::PointCloud2	publish

4.2.3 LV Builder

This node subscribes single topic published by the Data Fusion node. The main task of this node is to take the environment representation and reformat it into a suitable template that will be stored in a memory and compared with previously visited scenes. This node publishes a topic with the built template and two other topics for visualization and debugging purposes. Different approaches to the exact implementation of this node are described in the sections 4.4 - 4.7.

4.2.4 LV Matching

This node subscribes to a topic published by the LV Builder node. The goal of this node is to store all visited places, assign unique ids to all seen scenes, compare a received scene with other scenes, and decide if it was already seen. If the currently received scene template is similar enough to some of the stored templates, this node publishes the id of

¹Self defined message

Table 4.3: Subscribed and published topics by the LV Builder node

Topic	Type	Mode
rgb_cloud	sensor_msgs::PointCloud2	subscribe
current_scene_descripion	msgs::LVDescription ¹	publish
clustered_viz	sensor_msgs::PointCloud2	publish
convex_hull_viz	sensor_msgs::PointCloud2	publish

the matched template. If there is no such template, this node generates and publishes a brand new id and stores the received template as a newly visited place. The only topic this node is publishing is a topic with ids of matched or new scenes.

Table 4.4: Subscribed and published topics by the LV Matching node

Topic	Type	Mode
current_scene_descripion	msgs::LVDescription	subscribe
LocalView/Template	ratslam_ros::ViewTemplate	publish

4.2.5 Rat SLAM ROS

This diagram block represents not a single node but a whole package from several nodes. This is an OpenRatSLAM described in section 2.2, run without almost any changes. The only difference compared to the original package is the number of started nodes. The lv Node is not activated because its job is done by LV Builder and LV Matching node, and the visual odometry Node is replaced by an odometry sensor from the simulator. The package subscribes to the topic with scene ids published by the LV matching node and to the topic with odometry directly from the simulator. The only relevant published topic is the experience map topic, with the final experience map, which is the final result of the whole algorithm.

Table 4.5: Relevant subscribed and published topics by the RatSLAMRos package

Topic	Type	Mode
LocalView/Template	ratslam_ros::ViewTemplate	subscribe
odom	nav_msgs::Odometry	subscribe
ExperienceMap/Map	ratslam_ros::TopologicalMap	publish

4.2.6 LV Analyzer

This node subscribes to the same topics as the Rat SLAM ROS package. This node serves only debugging purposes and does not influence the algorithm. The goal of this node is to evaluate the performance of the algorithm. It receives all the ids of matched scenes and new ids from the LV Matching node and can pair them with the exact position of the robot at the time the scene template was taken because of the information received from the simulator. This node remembers the precise position of each scene newly remembered by the LV Matching node and can calculate the position difference between each match and the original matched scene. Furthermore, it can calculate the distance to the nearest previously visited scene for each newly added template. According to the metrics described in the section 5.2, the number of false positive and false negative matches can be calculated, leading to the approach's final accuracy, recall, and precision. These estimated numbers are the final output of this node.

Table 4.6: Subscribed topics by the LV Analyzer node

Topic	Type	Mode
LocalView/Template	ratslam_ros::ViewTemplate	subscribe
odom	nav_msgs::Odometry	subscribe
camera/rgb/image_raw	sensor_msgs::CompressedImage	subscribe

4.2.7 LV Dataset Creator

This node works in principle similarly to the LV Analyzer node. The goal of this node is to pair the templates with their exact positions received from the simulator. Unlike the LV Analyzer node, this node receives and pairs the whole template from the LV Builder node instead of only the scene id from the LV Matching node. The set of pairs of templates and their exact positions is the output of this node, which helps build final datasets for automatic parameter tuning, see section 4.5.3, or neural networks training, see section 4.6.2.

Table 4.7: Subscribed topics by the Dataset creator node

Topic	Type	Mode
current_scene_descripion	msgs::LVDescription	subscribe
odom	nav_msgs::Odometry	subscribe

4.3 Data Fusion and Preprocessing

This section introduces the process of processing the raw data received from the sensors and creating a final representation of the environment that is further used as an input for the other stages of the process.

In this thesis, we receive colored 2-dimensional images from an HD camera and a raw 3D point cloud from a 3D LiDAR sensor. The goal is to use these two inputs and generate a colored point cloud for a more accurate environment representation.

In this work, we assume that both sensors are calibrated and that the excentric parameters, namely field of view and transformation matrix between sensor's frames, are already known. If this is not the case, some of the following well-known techniques [44] [45] can be used for their determination.

The whole process can be divided into three major parts. In the beginning, the frequencies of the sensors must be synchronized. Then, after the input data are synchronized, the data fusion is performed, and the individual scene representations are merged into one mutual model, containing information from all individual sensors. Finally, the built representation is preprocessed and simplified by removing the unnecessary data, especially the information about the ground. The whole process is visualized in Figure 4.2 and each step is described in the following subsections.

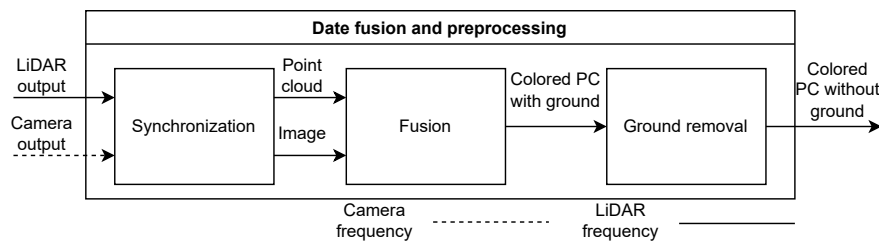


Figure 4.2: Data fusion workflow

Figure 4.3 illustrates example inputs received from the sensors, generated output after the data fusion, and final generated output after the ground removal.

4.3.1 Sensors Synchronization

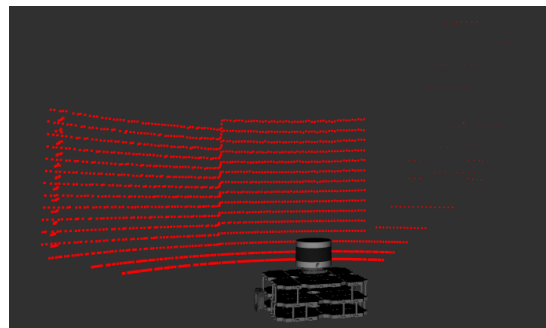
This section solves the problem that the sensors deliver data at different times with different frequencies. The goal of the synchronization is to receive unsynchronized data from both sensors and return synchronized pairs of images and point clouds that will be used for further fusion.

The technique used in this thesis is based on the assumption that the camera frequency is significantly larger than the frequency of the 3D-LiDAR². Based on this fact, the system can just record all the images received from the camera. All point clouds received from the 3D-LiDAR are afterward paired with the last received image.

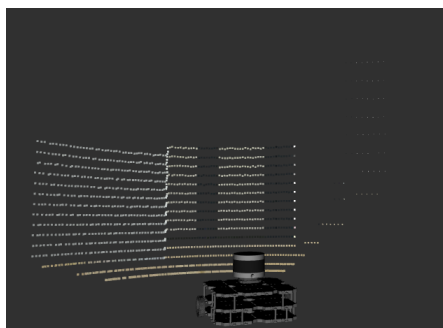
²In the experiments, we used a camera that has 15 times higher frequency than the 3D-LiDAR.



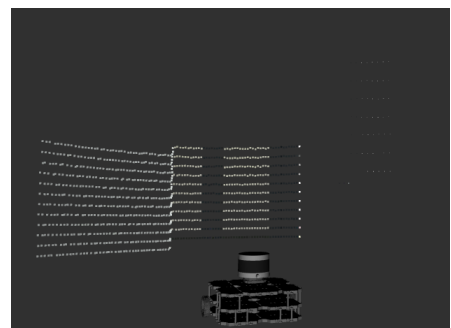
(a) Input received from the camera.



(b) Input received from the LiDAR.



(c) Colored point cloud after data fusion



(d) Final result after the ground removal

Figure 4.3: Data fusion sensors inputs and generated outputs after each stage

The time difference between the image and point cloud is so low, compared to the frequency of the LiDAR, that it can be neglected, and we can assume that the image and the point cloud were taken simultaneously.

4.3.2 Data Fusion

At this point, we assume that all the data are synchronized and working with a pair of images and raw point clouds representing the same scene at the same time. The goal is to build a colored 3D point cloud.

The point cloud PC is represented as an unordered set of triples, describing a single point's x, y, z coordinates:

$$PC \subseteq \{(x, y, z) | (x, y, z) \in \mathbb{R}^3\}.$$

The image can be represented as a function $img : \mathbb{R}^2 \rightarrow \mathbb{N}_0^3 \cup \{0\}$ taking x, y pixel coordinates as input and returning RGB representation of the pixels color or 0, if the give coordinates are out of range³:

$$img(x, y) = \begin{cases} (r, g, b) & \text{if } (x, y) \text{ are inside of the cameras field of view} \\ 0 & \text{otherwise,} \end{cases}$$

where r, g, b corresponds to the pixel color's red, green, and blue parts.

The result CPC will be represented as an unordered set of sextuplets, describing a single point's x, y, z coordinates together with r, g, b colors:

$$CPC \subseteq \{(x, y, z, r, g, b) | (x, y, z, r, g, b) \in \mathbb{R}^3 \times \mathbb{N}_0^3\}.$$

Let \mathbf{P} be the projection matrix that projects 3D world coordinates into the 2D pixel coordinates on the image plane using the following formula:

$$\mathbf{x} = \mathbf{P}\mathbf{X},$$

where $\mathbf{X} = [x_{\text{world}}, y_{\text{world}}, z_{\text{world}}]^T$ represents a 3D world coordinates vector and $\mathbf{x} = [x_{\text{image}}, y_{\text{image}}]^T$ represents a 2D image plane coordinates vector. This matrix can be found using the camera's and LiDAR's excentric parameters received from the calibration. [46]

If we know the projection matrix \mathbf{P} , we can iterate through all the points in the point cloud, project them into the image plane, find the corresponding pixel and bind its color with the examined point. All points outside the camera's field of view shall be ignored and not included in the result.

The algorithm for the fusion of the data received from LiDAR and camera is summarized in the Algorithm 1.

³If x or y are not the whole numbers, they are rounded to the nearest whole number.

Algorithm 1 LiDAR and camera data fusion**Input:** Point cloud PC , camera image img **Output:** Colored point cloud CPC

```

 $CPC := \{\}$                                  $\triangleright$  Initialize result as an empty set
 $P \leftarrow$  build projection matrix
for  $(x, y, z) \in PC$  do                 $\triangleright$  Iterate through all points in  $PC$ 
     $[x_i, y_i]^T \leftarrow P \cdot [x, y, z]^T$        $\triangleright$  Project current point to the image plane
    if  $img(x_i, y_i) \neq 0$  then             $\triangleright$  Ignore points out of cameras field of view
         $(r, g, b) \leftarrow img(x_i, y_i)$            $\triangleright$  Get projected pixel color
         $CPC \leftarrow CPC \cup \{(x, y, z, r, g, b)\}$      $\triangleright$  Add colored point to the result
    end if
end for
return  $CPC$ 

```

4.3.3 Ground Removal

Ground removal is a widely used technique, applied by many algorithms working with 3D point clouds. Even if the information about the ground, particularly about the ground color, might help distinguish between two different scenes, the points representing the floor are usually in the same position for every scene and therefore carry a relatively small information value. Removing these points can significantly reduce the input size, with minimal loss of the information value, which can positively influence the algorithm's performance. Furthermore, the ground points may connect two completely separate objects and therefore have a negative influence on the scene segmentation or object detection algorithms.

Let's assume that all points from the point cloud are represented in the world's frame of reference and that y axis is orthogonal to the ground. Then, it is evident that there exists a threshold y_{th} , such that all points representing a ground have y coordinate lower or equal to the y_{th} and all other points will have y coordinate larger than y_{th} . So, if the threshold y_{th} is known⁴, the ground point can be removed simply by filtering the points by their y coordinate. The ground removal process is summarized in the Algorithm 2.

Besides the ground, this method can remove some other objects' bottom parts, like the feet of pedestrians, wheels of wheelchairs, etc., which can lead to a slightly more significant information loss than pure ground removal. However, there exist other, better ground removal techniques, usually based on machine learning, which do not suffer from this issue [47] [48]. Yet, these techniques typically require more computational resources than the simple filtering approach, and the results are usually not significantly different⁵, so we decided to prefer this simple method despite the minor quality drawbacks.

⁴This threshold can be very easily determined experimentally.

⁵Especially in the indoor environments with static objects like furniture, which are in the main focus of this work

Algorithm 2 Ground removal

Input: Colored point cloud CPC , threshold y_{th}

Output: Colored point cloud CPC_2 without ground

```

 $CPC_2 := \{\}$                                 ▷ Initialize result as an empty set
for  $(x, y, z, r, g, b) \in CPC$  do          ▷ Iterate through all points in  $CPC$ 
    if  $y > y_{th}$  then                      ▷ Ignore points under the threshold
         $CPC_2 \leftarrow CPC_2 \cup \{(x, y, z, r, g, b)\}$  ▷ Add current point to the result
    end if
end for
return  $CPC_2$ 

```

4.4 General Scene Recognition Outline

After the data are fused into a uniform scene representation, the scene recognition is performed. This algorithm aims to remember all scenes the robot has visited and to decide if the current scene, received from the sensors, has been already visited or not, and eventually return the unique identification of the previously visited scene.

In order to achieve this goal, we need to find a suitable representation (further template) of the scene that will be remembered by the robot. This template must be created from the fused scene description received from the sensors, should occupy little space, and be easy to compare.

The scene recognition algorithm works in three steps. In the first step, the designed template is built from the received fused scene representation. In the second step, this template is independently compared with all the stored templates, representing previously visited scenes. A template comparison result is a real number between 0 and 1, representing the similarity of both templates. The closer the similarity to 1, the more similar the templates are. After all the templates are compared, the most similar template is chosen. In the last step, the similarity of the most similar template is compared to the given threshold. If it is greater, the most similar template is returned as the same scene. If it is smaller, the current template will be remembered, and the result will be that this scene was not visited before. The whole process is visualized in Figure 4.4.

The following sections suggest three different approaches to scene recognition. All presented techniques differ in template structures and template building and comparison algorithms. Otherwise, they all share the same structure shown in this section.

4.5 Hierarchical View Matching Based on Clustering

The first scene recognition method presented in this work found inspiration in the human memory of places. Unlike the further proposed methods, this approach does not try to model the brain's other biological structures but tries to conceive biological

4.5 Hierarchical View Matching Based on Clustering

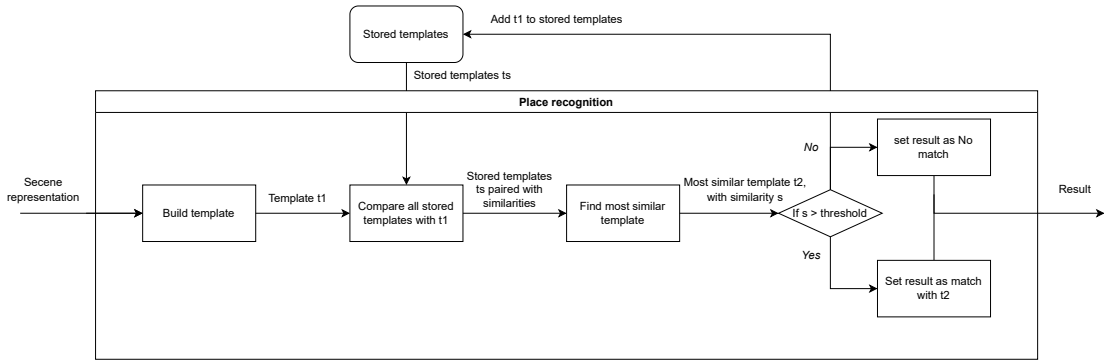


Figure 4.4: Common scene recognition workflow

inspiration more abstractly. The idea is based on the way how humans usually remember places. According to the [49], the long-term human spatial memory recall is built upon a hierarchical structure. First, people remember the general layout of the view. Afterward, they can recall basic information about the scene's largest or most significant features, followed by a few more detailed features. Finally, the small details are usually wholly forgotten or recalled at last.

The template representation used is based on this behavior. The scene is decomposed into a set of objects based on their location, connection, and color. Each object is simplified as a list of its most significant features, namely the position of its center point, volume and area of its convex hull, and its most significant color. Together with this information, the number of points from the colored point cloud in this object is stored. Afterward, the small, insignificant objects are entirely ignored.

During the matching process, the scenes are compared according to these objects. Objects are paired by their similarities based on their stored properties' similarities. The final similarity is calculated as a weighted average of these similarities by the number of points connected with the object. In this way, the largest, usually most significant objects influence the result more than the smaller details. An example of a scene's representation is shown in Figure 4.5

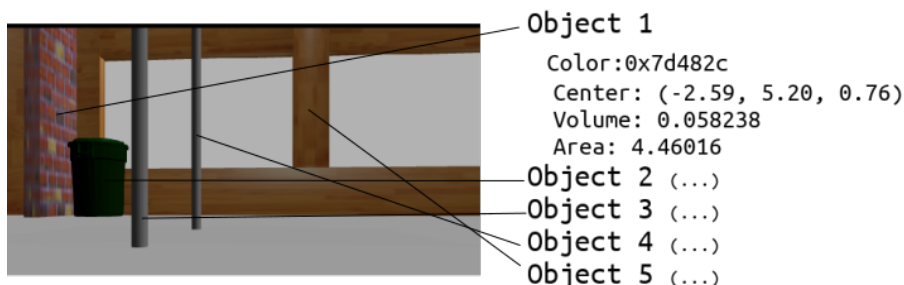
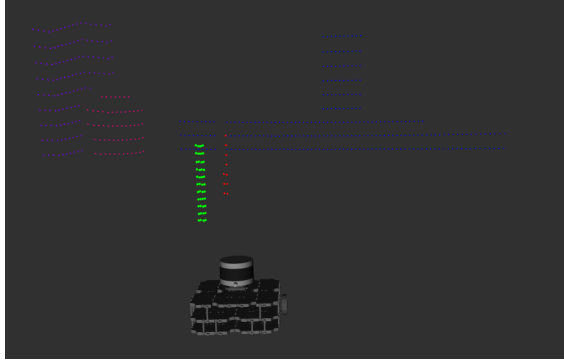


Figure 4.5: An example of the representation of a scene using clustering based approach



(a) Image of the scene



(b) Result of the clustering algorithm

Figure 4.6: Example of the clustered scene after applying the DBScan algorithm

4.5.1 Template Extraction

The decomposition of the colored point cloud into the set of objects description is a two-step process. In the first step, the scene is decomposed into clusters, representing individual objects. Afterward, in the second step, all clusters are processed independently, and the objects' information is extracted.

The clustering is performed using the DBScan algorithm [50] in a six-dimensional space. The first three dimensions standardly represent the points' x, y, and z coordinates. The additional three dimensions represent points' colors, namely the red, green, and blue components. The standard DBScan algorithm assumes that all dimensions are in the same units. Because there is obviously no standard conversion between color and distance, the color dimensions must be scaled by a suitable scaling factor. The best coefficient has been found experimentally, as well as the DBScan parameters. An example of the scene after clustering is displayed in the Figure 4.6a.

After the scene is decomposed, each cluster is processed independently of the others. Before the information about the object is extracted, its convex hull is found using the quick-hull algorithm [51]. After the convex hull is known, its center, volume, and area can be easily calculated. Together with the information obtained from the convex hull, the information about the object's color is extracted. Based on the properties of the

DBScan algorithm, it can be expected that all points from the cluster have a similar color. Therefore, storing average color instead of all individual colors leads to negligible information loss. The average color is calculated as an arithmetic average of the red, green, and blue parts of the colors of individual points in the cluster. After calculating, the average color is converted into the chosen color format. The last stored information about the object is the cluster size⁶.

All clusters with a size smaller than the given threshold are considered small insignificant objects and are ignored even before the object information extraction process starts. The scene decomposition process is visualized in Figure 4.7.

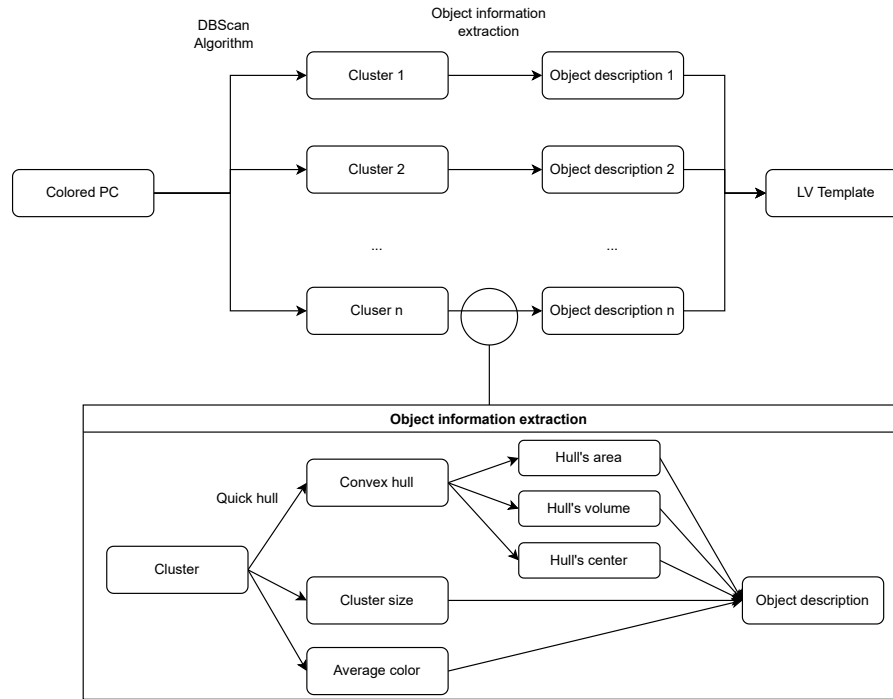


Figure 4.7: A scheme of the whole local view extraction process

4.5.2 Template Matching

Before calculating the similarity between two whole scenes, we need to describe an approach for comparison of two objects based only on the object properties. We compare four essential properties of the objects: distance between objects, the difference between colors, sizes, and shapes of the objects. The distance of the objects is calculated as the euclidean distance of their centers. The formulas described in section 3.8 are used for the color differences. The size difference is calculated as a difference between the volume of the convex hulls of the objects. For the determination and comparison of the exact shapes, we do not have enough information. However, much information about the

⁶Number of points in the cluster

4 Methodology

shape of many objects is encoded in a ratio between their volume and area. There are, of course, objects with entirely different shapes but similar ratios between volume and area, but for most pairs with different shapes, the ratio between volume and area is also different. So the difference between shapes is represented as a difference in the ratio of volume and area of the convex hulls of the objects.

At this point, the absolute difference between objects is known for each essential property, and we have to decide if they are similar enough or not. Therefore the function is needed for each property that takes the property difference as an input and returns a number between 0 and 1, representing the similarity of the individual property. In this work, we choose

$$f_{a,x_0}(x) = 1 - \frac{1}{1 + e^{-a(x-x_0)}}$$

as the wanted function for each property, where x is the input, and a and x_0 are parameters specific for each property. This function, illustrated in Figure 4.8, has a property that for differences smaller than the threshold, it is very close to one, for differences larger than the threshold, it is close to 0, and for inputs in the neighborhood of the threshold, it is gradually decreasing. The way how to find the suitable parameters is described in the following section.

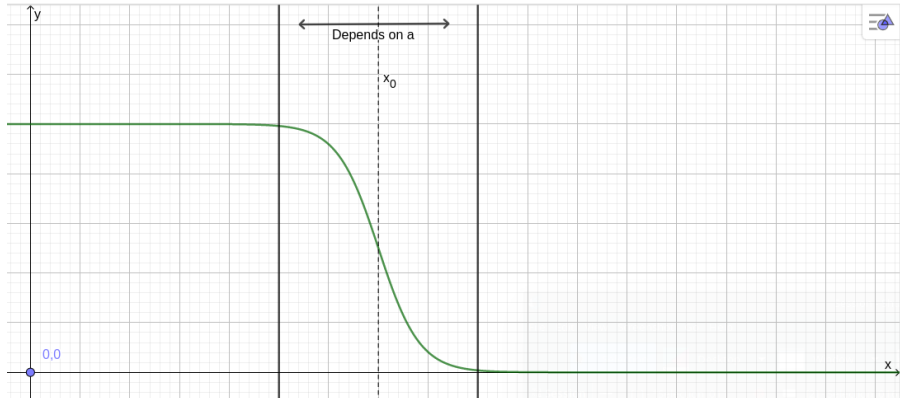


Figure 4.8: Parametrized sigmoid function

After the similarity of each property is calculated, the final similarity of the objects is calculated as a weighted average of the similarities of the individual properties. The weights are found automatically, as described in the following section. The object matching process is summarized in Algorithm 3.

The method for comparison of the two scenes uses the above-described approach for comparison of the individual objects. First, let's define a scene as an unordered set of objects. Then, let's define the primary scene as the current scene received from the sensors and the secondary scene as the scene from the storage. This approach iterates through all objects in the primary scene and, for each object, calculates the similarities with all objects in the secondary scene. Afterward, for each object in the primary scene,

Algorithm 3 Objects comparsion

Input: Objects O_1 and O_2

Output: Similarity of the objets

```

 $x_1 \leftarrow$  difference in colors between  $O_1$  and  $O_2$ 
 $x_2 \leftarrow$  difference in positions between  $O_1$  and  $O_2$ 
 $x_3 \leftarrow$  difference in volume between  $O_1$  and  $O_2$ 
 $x_4 \leftarrow$  difference in volume/area ration between  $O_1$  and  $O_2$ 
 $s_1 \leftarrow f_{a_1,x_{0,1}}(x_1)$ 
 $s_2 \leftarrow f_{a_2,x_{0,2}}(x_2)$ 
 $s_3 \leftarrow f_{a_3,x_{0,3}}(x_3)$ 
 $s_4 \leftarrow f_{a_4,x_{0,4}}(x_4)$ 
 $res \leftarrow \frac{w_1s_1+w_2s_2+w_3s_3+w_4s_4}{w_1+w_2+w_3+w_4}$ 
return res
    
```

the most similar object from the secondary scene is picked⁷. Finally, the similarities with the most similar objects are used to calculate the average, weighted by the sizes of the clusters. The whole process is summarized in the Algorithm 4.

Algorithm 4 Scenes comparsion

Input: Primary scene S_1 and secondary scene S_2

Output: Similarity of the scenes

```

res := 0
sizesTotal := 0
for  $o_1 \in S_1$  do
    best := 0
    for  $o_2 \in S_2$  do
        best  $\leftarrow$  max(best, CompareObjects( $o_1, o_2$ ))
    end for
    res  $\leftarrow$  left + best · clusterSize( $o_1$ )
    sizesTotal  $\leftarrow$  sizesTotal + clusterSize( $o_1$ )
end for
res  $\leftarrow$   $\frac{res}{sizesTotal}$ 
return res
    
```

4.5.3 Automatic Parameter Tuning

To make the templates comparison algorithm work, 13 different parameters must be correctly set. Namely, a and x_0 parameters for the sigmoid functions for each of four property differences, the weight of each property, and the final threshold. There are naturally many combinations, and every change may strongly influence the results

⁷Two objects in the primary scene may have the same most similar object from the secondary scene

and the optimal values of the other parameters, so manual setting of these parameters wouldn't bring satisfactory results. Therefore, an automatic optimization method that minimizes the number of errors based on the choice of the correct parameters is required.

In this work, we used genetic algorithms[52]. The minimized fitness function is a count of false positive and false negative evaluations after a simulation of a robot run in a prepared environment. The simulation, environments, and evaluation metrics are the same as those used for the performance testing and are described in sections 5.1 and 5.2. In some cases, like usage of the approach for the 2-Stage matching, see section 4.7, it might be beneficial to minimize the number of false positives at the expense of false negatives or vice versa. In this case, we can appropriately weigh the number of false positives and negatives in the final sum.

4.6 Neural Networks Based View Matching

The second technique offered in this work is based on neural networks. This approach is not designed as a standalone method but is presented only for better understanding and further used in the 2-Stage approach presented in the section 4.7. The used neural network is inspired by siamese neural networks [53].

These networks usually consist of two parts and are typically designed to compare any two entities. The first part consists of two networks with the same structure and usually with shared weights. This part is used for the automatic feature extraction from the input entities. The second part consists of a single network taking feature vectors extracted by both neural networks in the first part, performing the desired operation on the entities, and building corresponding output. In the case of comparison network is the output of the second part, and therefore of the whole network, a single number between 0 and 1, determining the similarity of the entities. The typical structure of a siamese neural network is shown in Figure 4.9.

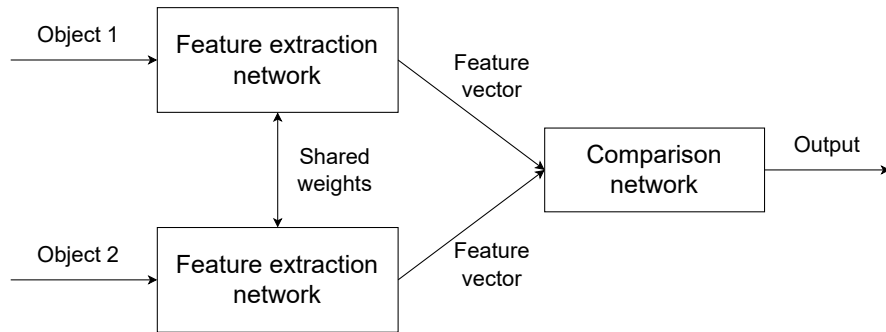


Figure 4.9: Example of a siamese network used for object comparison

4.6.1 Networks Structure

In this work, a slightly modified PointNet network, see section 3.7, is used as a feature extractor. The only modification compared to the original networks is in the sizes of the layers and the output because we are typically working with significantly more sparse point clouds than the network designers. As a result, the extracted feature vector contains only 256 numbers instead of 1024.

The feature vector extracted by this network is the scene template extracted from each input, processed in the future steps, and eventually stored in the storage.

The two extracted feature vectors are further compared by a single multilayer perceptron network (further MLP). This network has 512 input neurons and produces a single output. The network takes as input a concatenation of both feature vectors and produces a number between 0 and 1, describing the similarity of the scenes represented by given feature vectors. Several architectures of the networks were tried, but the best results were produced by a network with a single hidden layer containing 256 neurons and with a sigmoid as an activation function on the output neuron.

4.6.2 Training of the Networks

Both networks are trained separately. For the training of the PointNet, used for the feature extraction, we used an original algorithm presented in [37]. In order to be able to evaluate the results and compare them with the expected results in the dataset, the PointNet network was concatenated with a simple MLP network used for the object classification. Then, the whole classification network was trained on the PointNet40 [54] dataset. After the classification network was trained, the final MLP network was removed, and the first PointNet part was used as a trained model for the feature extraction.

The second part of the network, namely the MLP comparing two feature vectors, was trained using a backpropagation algorithm [55] based on the mean squared error loss function [56]. The dataset was generated from a sample simulation, see chapter 5. During the simulation, the trained feature extractor network creates a feature vector from each scene. Afterward, a set of all pairs of the feature vectors is made. A random subset was chosen from this set, and all couples from this subset were labeled using exact scene locations received from the simulator and the criteria described in the section 5.2. This labeled subset was used as a training set for the MLP network.

4.7 2-stage View Matching

This approach tries to combine both previously presented methods to achieve better results. The first approach works pretty well in many scenes but has one drawback. Since the objects' shapes are mainly ignored, taking into account only the ratio between the volume and the area of the objects, there could be many scenes with similarly placed objects with similar sizes but different shapes. This could lead to many unwanted false

positive evaluations. This approach tries to use neural networks presented in section 4.6 to eliminate these false positives while maintaining most of the advantages of the first approach, described in section 4.5.

4.7.1 Template Building

The scene representation in this method combines the scene representations from both previously presented techniques. The scene is represented as a set of objects description, as described in section 4.5, and simultaneously, the feature extraction described in section 4.6 is performed. The Final representation is a tuple of the object decomposition and features vector.

4.7.2 Template Matching

As the name of the approach suggests, the matching is performed in two stages. In the first stage, the similarity of the two scenes is calculated the same as in the section 4.5. After the similarity is computed, it is compared with a given threshold so that it is predecided, if it is positive or negative. The calculated similarity is returned as a final result if it is negative. If it is positive, the second stage is performed in order to reduce the number of false positives.

In the second stage, the feature vectors are compared in the same way as in a section 4.6. If the result is higher than another threshold, the result of the first stage is returned. If the result is lower than the threshold, 0 is returned. The whole process is summarized in Figure 4.10.

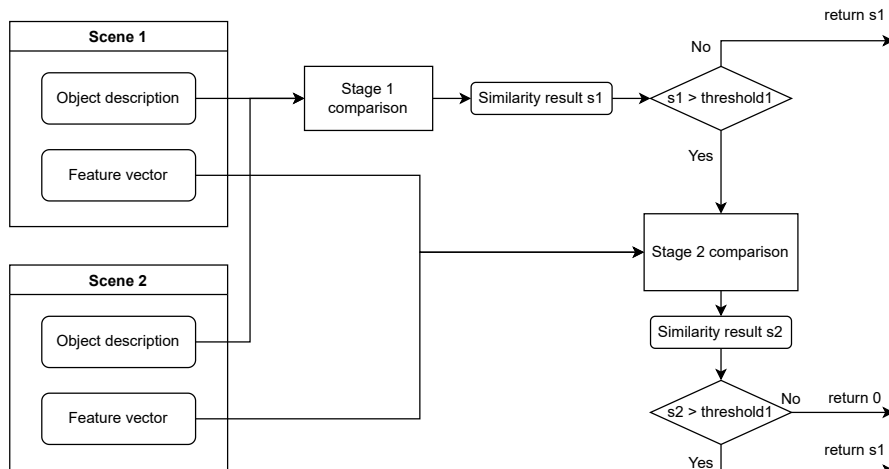


Figure 4.10: Overview of the two-stage approach

5 Experiments

In this section, all presented algorithms will be tested using different metrics and compared with the visual place recognition used in the OpenRatSLAM approach, described in section 2.2. The beginning of the chapter will introduce the robot simulator and the environments used for the tests. The following section formally defines the evaluation metrics. The next section will present the system setup of the experiments. In the following four sections, the results of the different evaluation metrics will be discussed. In the penultimate section will be tested the integration of the place recognition approaches with RatSLAM. Finally, the last section will summarize all measured results and discuss the final performance and advantages or disadvantages of all suggested techniques.

5.1 Used Environments

The system has been tested using a gazebo simulator, described in the section 3.2. As a robot model, the turtlebot3 waffle PI, described in section 3.3, was used and slightly modified with a 3D LiDAR sensor [57]. The most important parameters of the robot are summarized in the table 5.1.

Table 5.1: Turtlebot3 Waffle PI specification

width	height	depth	max speed	cam. frequency	LiDAR frequency
281 mm	141 mm	306 mm	0.69 ms ⁻¹	30 Hz	2 Hz

The robot has been tested in three different environments: Warehouse world [58], House world [59] and Hospital world [60].

The warehouse world, shown in Figure 5.1, is a representative environment for most industrial environments in which many robots find an application.

The House world, shown in Figure 5.2, represents a typical small, fully equipped apartment. Compared to the warehouse, this environment is significantly smaller and contains more various objects of different shapes and colors. Many of the typical household robots, like robotic vacuum cleaners, will deal with environments like this.

Finally, the hospital world, shown in Figure 5.3, is a large, mostly empty environment from the hospital building. This environment is mostly symmetric and contains many places that look very similar, even if they are at opposite building sites. This environment was included mainly to test the algorithm's robustness against these symmetric places. Furthermore, this environment is a typical representation of any office or similar public building.

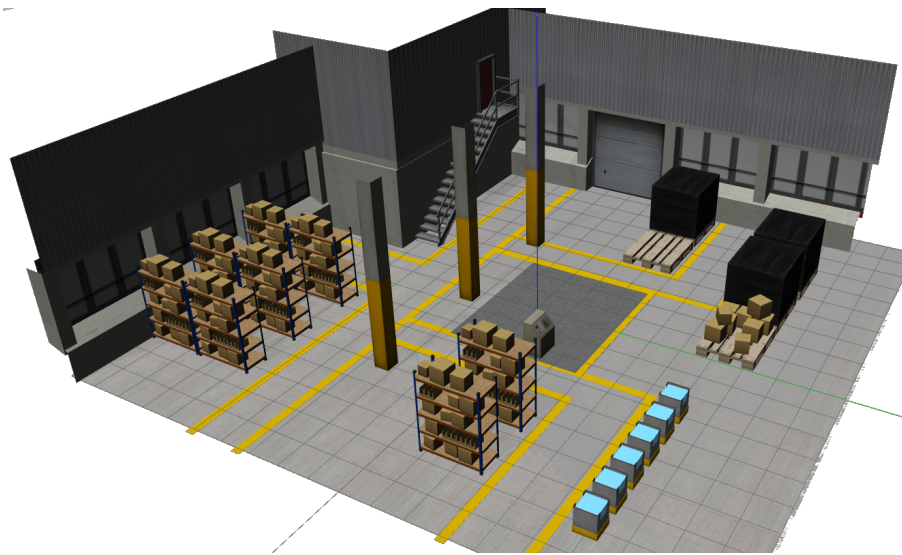


Figure 5.1: The warehouse world environment 5.1



Figure 5.2: The small house world environment 5.2

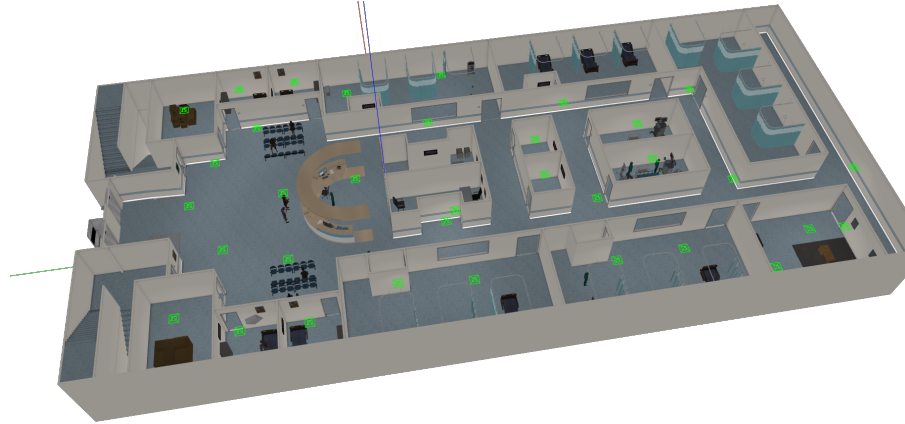


Figure 5.3: The hospital world environment 5.3

The algorithms were tested in each of the presented environments with several minutes long robot runs. The robot's trajectory was chosen so that the robot visits the same places several times to test the scene recognition algorithm properly. All the robot runs were saved in rosbag files to ensure the repeatability of each experiment. Furthermore, every experiment for every metric presented further in this chapter has been performed on the same trajectory.

The datasets generated for the parameter tuning, described in the section 4.5.3, and for the training of the neural networks, described in the section 4.6.2, were generated exclusively from the warehouse environment. The datasets' trajectory was entirely different from the trajectory used for the performance testing, but the type of the objects remained similar. In these datasets were no scenes from the other two environments.

5.2 Evaluation

The result of a place recognition for a single scene can be either positive or negative. The positive evaluation means that the scene matched one of the previous ones, and the negative means that this scene is entirely new. However, in contrast to many classification algorithms, the result strongly depends on the earlier results, and the evaluation order of scenes matters. Furthermore, the classification algorithms generate the ids of the scenes instead of the direct positive/negative evaluation.

Let n be number of scenes in the simulation and $S = (s_1, s_2, \dots, s_n)$ an ordered set of scenes that are gradually passed as an input to the algorithm. Let $P = (p_1, p_2, \dots, p_n)$ be an ordered set of the exact robot locations¹ and $O = (o_1, o_2, \dots, o_n)$ be an ordered set of exact robot orientations, on which the robot was in a time, when the appropriate scene was taken. Finally, let $R = (r_1, r_2, \dots, r_n)$ be an ordered set of scene ids, generated as an output of the place recognition algorithm.

¹ x and y coordinates

Now, the result r_i will be considered positive if

$$\exists j < i : r_j = r_i,$$

and negative if

$$\forall j < i : r_j \neq r_i.$$

The positive result is considered a false positive if the first scene with the same id is too far from the current scene in terms of location and orientation. The negative result is considered false negative if a previously saved scene is very close to the current scene in terms of location and orientation.

Formally, let

$$first_ind(x) = \begin{cases} i \text{ st. } r_i = x \wedge \forall j < i : r_j \neq x & \text{if } x \in R \\ 0 & \text{otherwise} \end{cases}$$

be a function that returns the index of the first scene evaluated with an id x . Let r_i be a positive result. r_i is a false positive if and only if

$$\|p_{first_ind(r_i)} - p_i\| > th_{pos1} \vee |o_{first_ind(r_i)} - o_i| > th_{ori1}.$$

Now let r_i be a negative result. r_i is a false negative if and only if

$$\exists x < r_i : \|p_{first_ind(x)} - p_i\| \leq th_{pos2} \wedge |o_{first_ind(x)} - o_i| \leq th_{ori2}.$$

The thresholds depend on the resolution of the cell network used in the RatSLAM algorithm. Based on the robot's dimensions, the place cell size was chosen as 20 cm, slightly smaller than the robot. If the positively evaluated location is close enough, e.g., in the neighboring cells as the matched location, the algorithm still works well. Because of this, the false positive position threshold th_{pos1} was chosen as 80 cm, which is more than four cells away. Similarly, the size of orientation cells is 12°, and the false positive threshold th_{pos2} was chosen as ca 22.9183°.

The false negative thresholds were chosen the same as the cell sizes, so 20 cm and 12°.

5.3 System Setup

The system's performance has to be measured without influencing the program's run. This purpose serves the Node LVAalyzer, which only subscribes to several topics and does not publish any messages. This node performs the complete performance analysis of the system.

This node contains a class Analyser, which performs the entire analysis. After the initialization, the class can be used by repeatedly calling its method insert. This method takes an id of a newly classified scene together with the robot's position and orientation at the scene's time. If the id is new, the position and orientation are stored, and

all previously stored positions and orientations are compared to detect possible false negative. If the id already exists, the current position and orientation are compared with the stored one to detect possible false positive evaluation.

If the insert method is called on all scenes during the algorithm's run, the total number of true and false positives and a total number of true and false negatives is calculated. Furthermore, the analyzer generates detailed information, like ids, time, and exact positions of all false positive and negative evaluations. In addition to that, if the scene images are passed as a third optional parameter to the insert method, the Analyser will generate images of all false positive evaluations to see the difference between the wrongly matched views. This class also provides an animated live preview of all the scenes and their matches, as shown in Figure 5.4.



Figure 5.4: Preview of the animation generated by the analyzer. The left part shows a current scene and position, and the right part shows the preview of a matched scene.

The LVAnalyzer node is a wrapper over the Analyser class. This node subscribes to three topics, LVTtemplate, Odometry, and Camera. After receiving a new matched template id from the LVTtemplate topic, the exact position and scene image is found from the Odometry and Camera topics based on the timestamp of the messages. Afterward, all information is passed to the Analyser class using the insert method.

5.4 Accuracy

One of the essential evaluation metrics is the algorithm's accuracy, which will be measured in this section. In the beginning, the approaches presented in sections 4.5 and 4.7 will be compared using PR curves in all three environments. Afterward, the best thresholds will be picked, and the final accuracy measured for both approaches and compared with the accuracy of the visual matching used in the OpenRatSLAM.

The thresholds are one of the factors that influence the results the most. To find the best threshold values and to adequately compare both techniques, the accuracy, recall, and precision were measured for all possible threshold combinations with 0.01 steps. The measured values for all different thresholds were used to build the PR curves,

5 Experiments

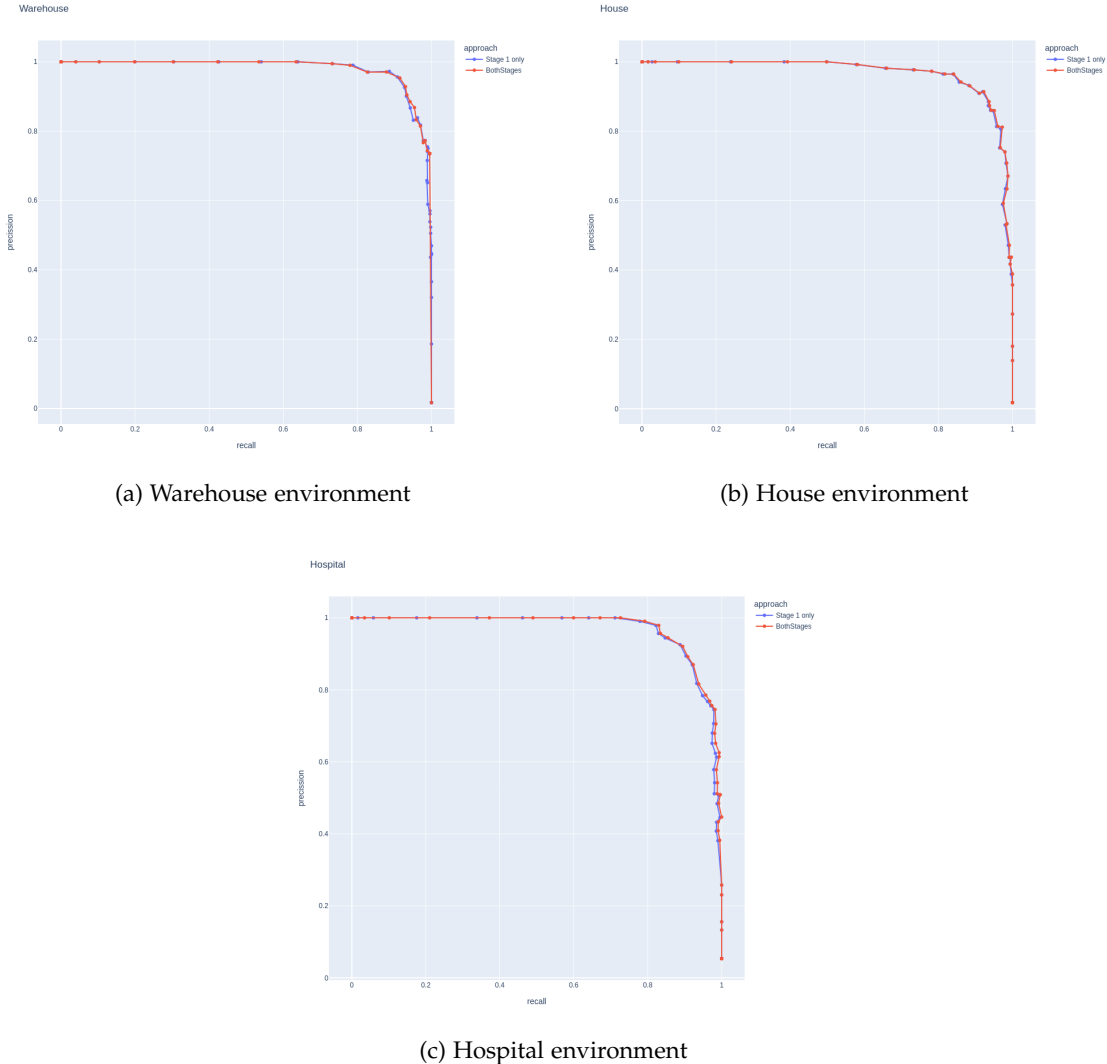


Figure 5.5: PR Curves comparing Hierarchical and 2-Stage view matching approaches

presented in Figure 5.5.

Because the thresholds influence only the LV matching part and not the LV building part, the local views were built and saved using the LV Dataset creator node, presented in section 4.2.7. This dataset was afterward used for evaluation instead of running the whole simulation, which saved a lot of time.

As Figure 5.5 shows, both approaches have very similar results. Still, the method with two stages slightly outperforms the hierarchical approach with only the first stage by eliminating some false positive evaluations. Examples of false positives, evaluated by the first stage and eliminated by the second stage, are shown in Figure 5.6.

After the optimal thresholds were picked, the overall accuracy of both approaches



Figure 5.6: Examples of false positives eliminated by the second stage

was measured and compared with the accuracy of the visual place recognition used in the OpenRatSLAM. The results are shown in the table 5.2.

Table 5.2: Accuracy of all approaches in different environments

	1st stage only	both stages	OpenRatSLAM
Warehouse	88.84 %	89.28 %	77.67 %
House	86.69 %	86.94 %	41.25 %
Hospital	86.19 %	86.38 %	79.36 %

As the results show, both approaches have very similar results in all environments, but the method with both stages still slightly outperformed the technique with only the first stage. We can also see that both suggested approaches significantly outperformed the visual place recognition used in the OpenRatSLAM version in every environment, especially in the house world. Furthermore, the experiment results proved the ability to generalize on the environments diametrically different from the warehouse environment used for the model training.

5 Experiments

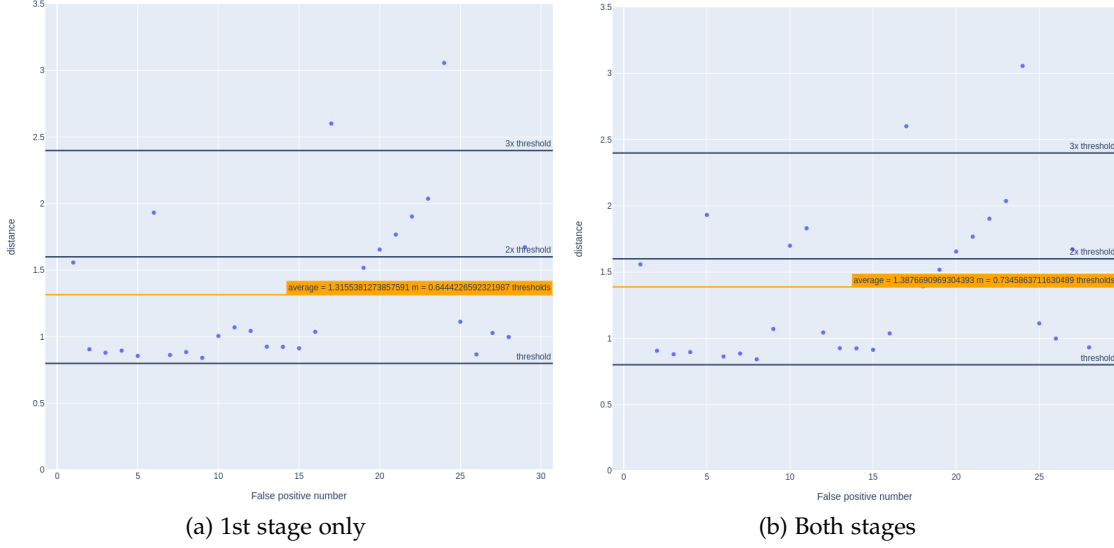


Figure 5.7: False positive distances in the warehouse environment

5.5 Average False Positive Error

Apart from the number of false positive and false negative evaluations, the distances of the false positives between the wrongly estimated scenes is another critical performance metric. If the false positive is close to the threshold and the distance is relatively small, then the result won't be influenced much. However, if the distance between wrongly matched scenes is very large, the negative impact on the result will be significant.

This section analyzes distances for every false positive result during the simulation in every environment. The exact distances for every false positive evaluation for both approaches are shown in Figures 5.7, 5.8, and 5.9. The average and maximal error distance for each approach in each environment, together with the comparison with the visual place recognition used in the OpenRatSLAM, is shown in the table 5.3.

Table 5.3: Average and maximal errors of false positive evaluations in different environments

	1st stage only		both stages		OpenRatSLAM	
	avg	max	avg	max	avg	max
Warehouse	1.32 m	3.06 m	1.39 m	3.06 m	8.93 m	11.52 m
House	0.93 m	1.16 m	0.99 m	1.39 m	1.84 m	3.93 m
Hospital	1.00 m	1.52 m	1.00 m	1.51 m	6.56 m	14.57 m

As the results show, both techniques suggested in this work showed outstanding performance in this metric. In the house and hospital environment, the average error lies only 13-20 cm away from the threshold, which is less than 25 % of the threshold size.

5.5 Average False Positive Error

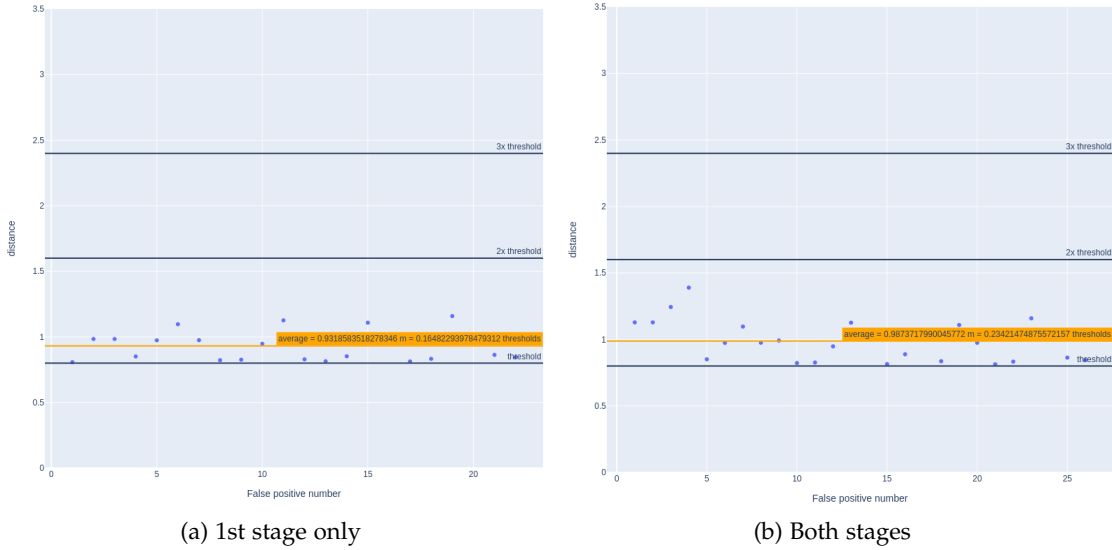


Figure 5.8: False positive distances in the house environment

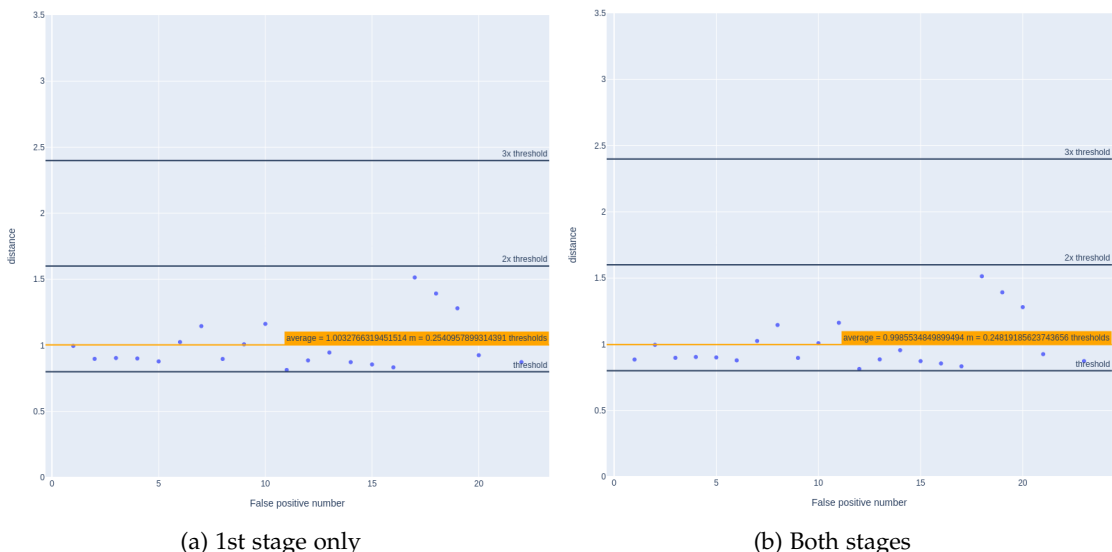


Figure 5.9: False positive distances in the hospital environment

Moreover, all evaluated false negatives in these environments are not farther than twice the threshold from the matched scene. This means that all wrongly evaluated matches are still very close to the threshold and shouldn't cause almost any damage to the final result. Some errors in the warehouse environment were slightly larger, but they were only exceptional cases, and most of the wrongly classified matches are still very close to the threshold.

On the other hand, the results of the visual place recognition used in the OpenRat-SLAM were significantly worse. As the results suggest, most of the wrongly evaluated scenes were spread over the whole environment, and the distances between the incorrectly matched scenes were huge. The most significant errors can be observed in the hospital environment, which drastically influenced the generated experience map, as discussed in the section 5.8.

According to this metric, both presented approaches significantly outperformed the visual place recognition used in the original RatSLAM.

5.6 Time Performance

Another important property is the time of the local view template building and especially the time of comparing two templates. The time of the template building and comparing the two templates are measured separately. The reason is that the template building is done only once per scene, independently of the length of the algorithm's run. However, comparing the two templates is done more times for every scene. Namely, every new scene is compared with all previously saved scenes whose number increases over time, especially in large and various environments. Therefore, the time of the matching is the critical part and must be as fast as possible. In contrast, the time of the building can be significantly larger as long as it stays smaller than the period between two sensor inputs.

The system was tested on a Laptop with the following parameters:

Processor: Intel® Core™ i7-8650U Processor (1.9 - 4.2 GHz)²

RAM:

- 4 GiB Row of chips DDR4 Synchronous Unbuffered (Unregistered) 2400 MHz (0,4 ns)
- 8 GiB SODIMM DDR4 Synchronous Unbuffered (Unregistered) 2400 MHz (0,4 ns)

OS: Kubuntu 21.10 x86_64,

inside of the virtual machine, with the following limitations and operating system:

RAM: 8 GiB

OS: Ubuntu 20.04 LTS x86_64.

²<https://ark.intel.com/content/www/us/en/ark/products/124968/intel-core-i7-8650u-processor-8m-cache-up-to-4-20-ghz.html>

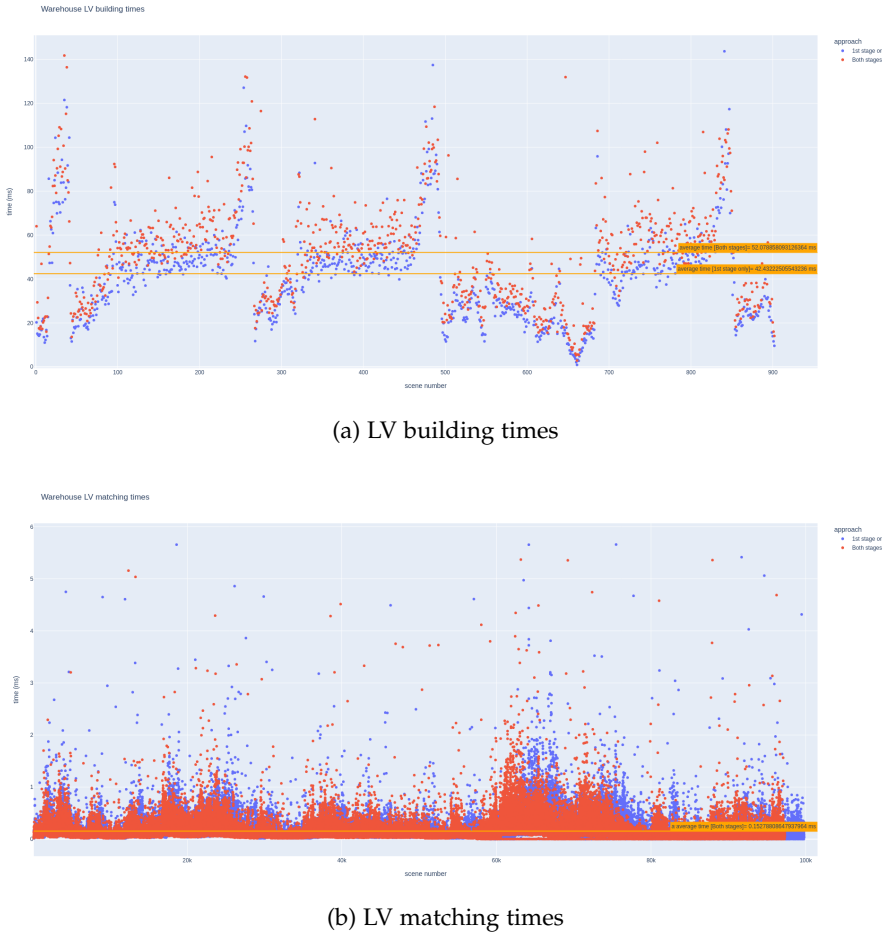


Figure 5.10: Computation times in the warehouse environment

The GPU did not have CUDA support, so all the computations were performed on a CPU.

Figures 5.10, 5.11, and 5.12 show the LV building times for each scene and also matching times for each pair of compared scenes in all the environments. The table 5.4 shows the average times for each approach in every environment compared with the visual place recognition used in the OpenRatSLAM.

The table and graphs show that the approach that uses only the first stage can build the local views considerably faster than the 2-stage approach. The time difference is caused by the feature extraction, which is present only in the 2-stage approach. However, the time difference is not so significant. Most importantly, the techniques are significantly faster than the frequency of the sensors, so the time performance of local view building of both methods is satisfactory. As we can see, the LV building is significantly slower than the LV building in the OpenRatSLAM. However, the OpenRatSLAM works with sensors

5 Experiments

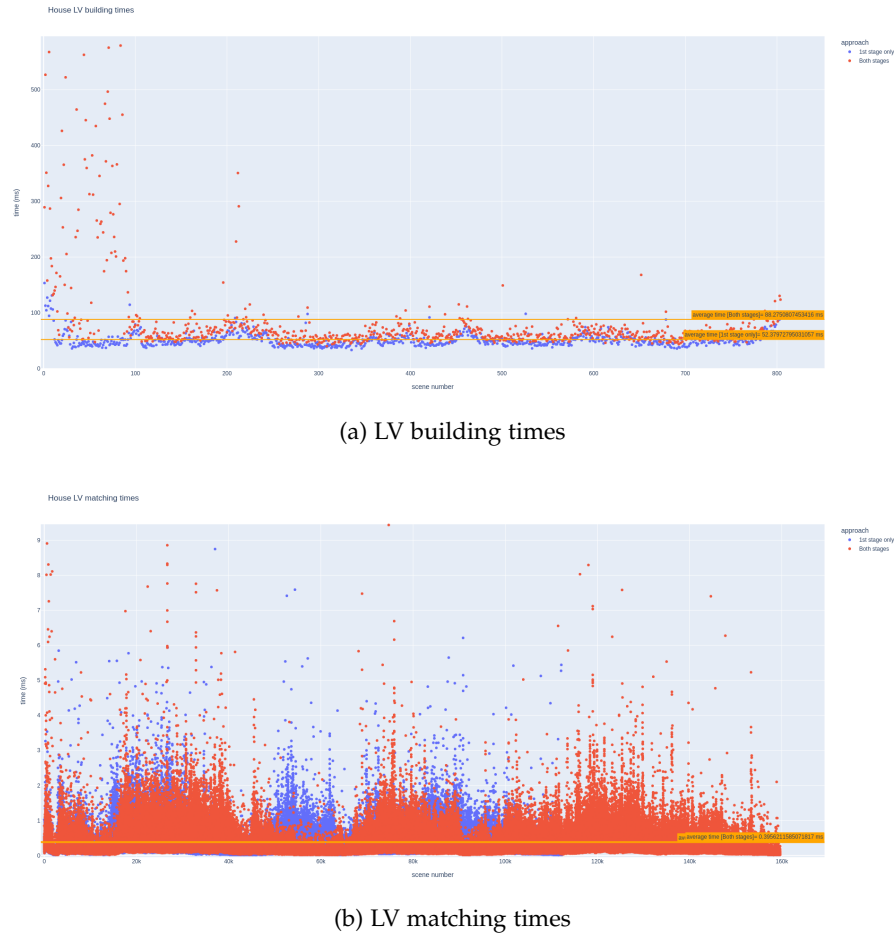


Figure 5.11: Computation times in the house environment

Table 5.4: Average times of LV matching and building in the different environments

	1st stage only		both stages		OpenRatSLAM	
	build	match	build	match	build	match
Warehouse	42.432 ms	0.153 ms	52.078 ms	0.159 ms	2.053 ms	0.083 ms
House	52.380 ms	0.396 ms	88.265 ms	0.368 ms	1.448 ms	0.137 ms
Hospital	55.271 ms	0.399 ms	65.609 ms	0.409 ms	1.762 ms	0.092 ms

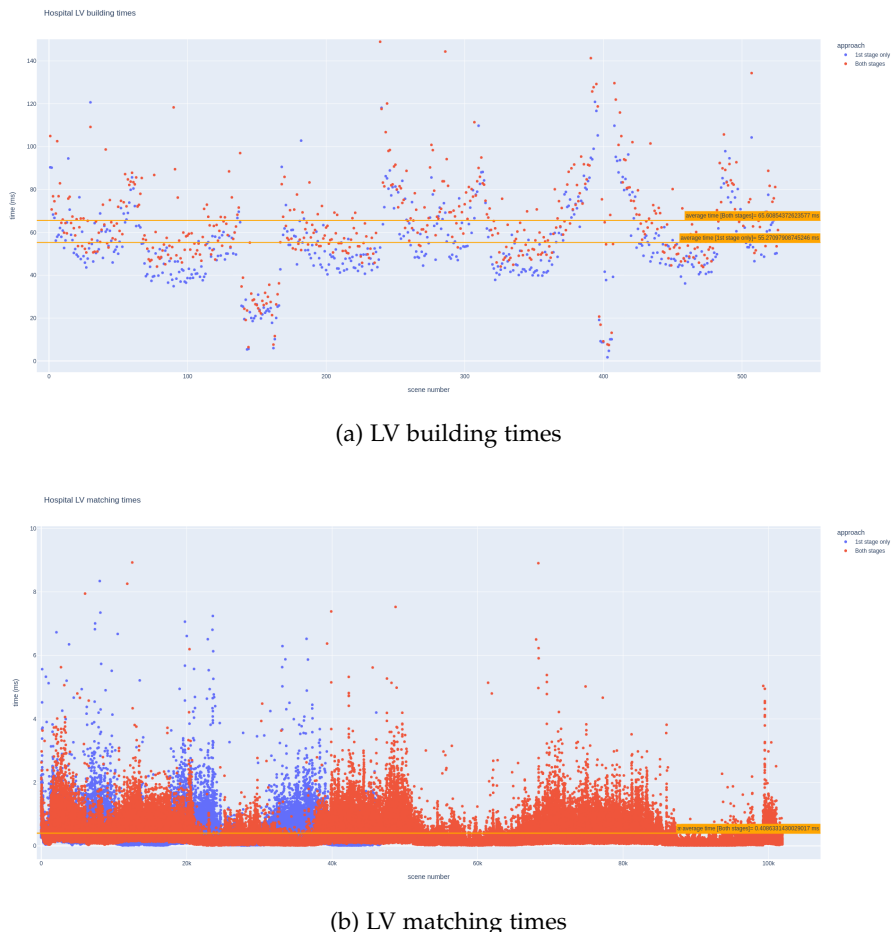


Figure 5.12: Computation times in the hospital environment

with significantly higher frequency³, so the LV building is done significantly more often, and the total resources consumption of the LV building process is comparable with the total consumption of the approaches presented in this work.

The times of the view matching of both approaches are almost the same, so the overhead caused by feature comparison in the second stage is practically negligible. Even if the times are circa 2 to 4 times larger than the times measured by the OpenRatSLAM, the number of saved views is significantly smaller, as shown in table 5.5, so the total comparison time for each scene will be at the end smaller than in the OpenRatSLAM approach. Furthermore, the times are significantly smaller than 1 ms, so there could be saved up to a thousand different local views to compare until the total comparison time reaches the sensors period. This means that this approach will also be suitable for very long time runs in huge environments.

5.7 Memory Consumption

Especially for the robots with low-performant controllers, for example, older Raspberry PI, RAM is a very limited resource, so the memory needed for storing the local views needs to be as small as possible. Therefore another metric evaluated in the algorithms is the consumption of the memory. The measurement results are shown in the table 5.5.

Table 5.5: Average memory consumption of the algorithms in the different environments

	1st stage only		both stages		OpenRatSLAM	
	\emptyset LV size	\emptyset LVs stored	\emptyset LV size	\emptyset LVs st.	\emptyset LV size	\emptyset LVs st.
Warehouse	78 B	194	1102 B	191	600 B	312
House	128 B	219	1152 B	216	600 B	445
Hospital	130 B	151	1154 B	148	600 B	219

The OpenRatSLAM uses a compressed 60x10 pixels big grayscale image as a local view template, so the memory needed for storing a single local view is always constant. However, the memory required for storing a single LV in the approaches suggested in this work differs for each local view and depends on the number of clusters detected by the DBScan algorithm. The difference between the size of the LV templates used in the approach with only the first stage and with both stages differs by a feature vector of 256 floating point numbers. Therefore, as follows from the table, the memory consumption of the first stage-only approach is significantly smaller than while also using the second stage.

The memory needed for storing the local views using the 2-stage approach is, on average, almost twice as large as the memory required for storing the lv template in the OpenRatSLAM approach. However, the number of stored templates in the OpenRatSLAM is almost twice larger than the number of stored templates in the 2-stage

³In the experiments, the frequency of the camera was 15 times higher than frequency of the LiDAR.

approach, so the total memory consumption remains similar. More interesting is the algorithm with only the first stage, in which a single local view consumes about six times less memory than the OpenRatSLAM approach. Furthermore, this approach stored, on average, significantly fewer local views than the OpenRatSLAM algorithm, so the total memory consumption is up to 12 times lower than in the OpenRatSLAM.

5.8 RatSLAM Integration

The last metric to test is the integration with the RatSLAM. This section will integrate the scene recognition algorithm with the RatSLAM ROS system, generating the final experience maps. Finally, the maps generated for both approaches will be compared with the exact trajectory generated by the simulator and the experience map generated by the OpenRatSLAM with only visual scene recognition.

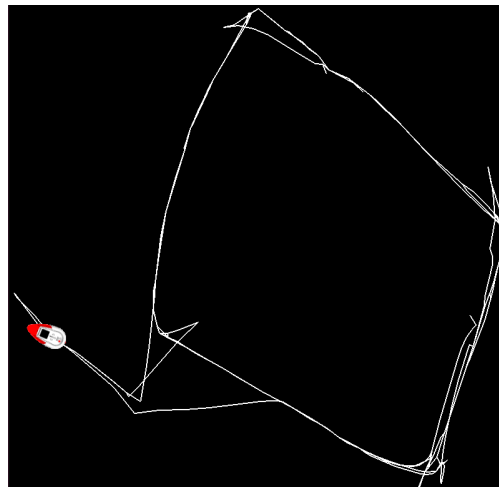
Even if the other evaluation techniques proved the significantly better performance of the methods suggested in this work, it is unclear if they will produce satisfactory results in connection with the RatSLAM, primarily because of the significantly lower frequency of the sensors. Therefore, this section aims to show that the improved performance compensates for the frequency loss of the sensors and that the generated results are at least as good as the results produced by the OpenRatSLAM or even better.

Figures 5.13, 5.14, and 5.15 show the generated experience maps by every approach, including the OpenRatSLAM, together with the exact trajectory. The pictures clearly show that the results generated by the approaches with only the first stage and with both stages are almost identical. Even if the accuracy of the 2-stage approach was slightly better, the difference was too small to influence the results of the RatSLAM algorithm significantly. However, after comparing the generated maps with the exact trajectory, we can see that the results are satisfactory and that the suggested approaches are fully compatible with the RatSLAM algorithm.

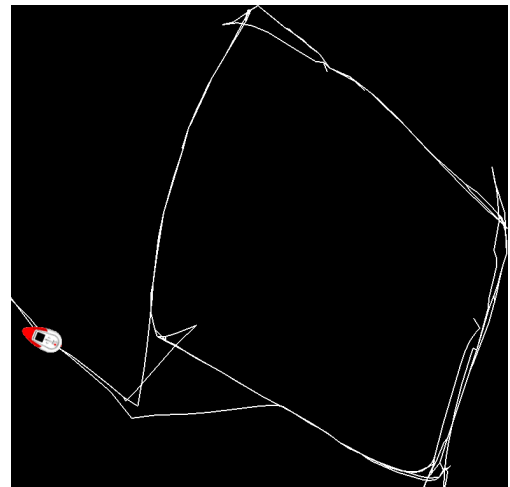
Furthermore, the results from the hospital environment presented in Figure 5.15 clearly show that the suggested approaches can outperform the OpenRatSLAM even in the generated trajectories. Because of the symmetry of the environment, the false evaluations of the visual scene recognition approach influenced the generated trajectory so significantly that it was entirely different from the exact one, and therefore, the OpenRatSLAM algorithm completely failed. However, the LiDAR sensors are considerably more precise in object distance estimation than a camera image, so the symmetry of the environment did not cause so many problems, and the generated results from the approaches suggested in this thesis were satisfactory.

5.9 Discussion

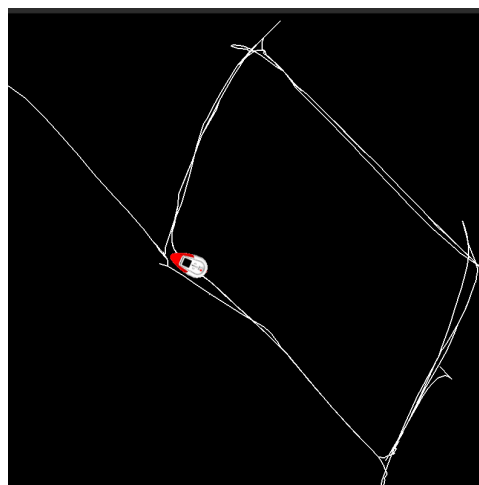
Both suggested algorithms were tested for performance in different aspects in different environments and showed satisfactory results in every measured evaluation metric. Surprisingly, the approach that uses only the first stage of the place recognition process



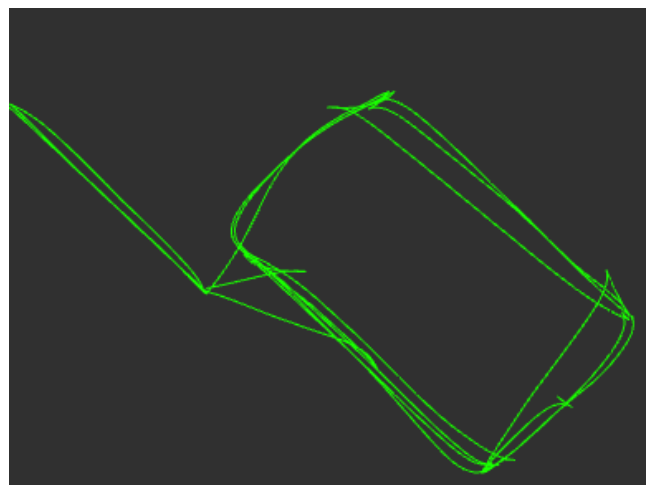
(a) 1st Stage only approaches



(b) Both stages approaches



(c) OpenRatSLAM



(d) Exact trajectory

Figure 5.13: Generated experience maps in the warehouse environment

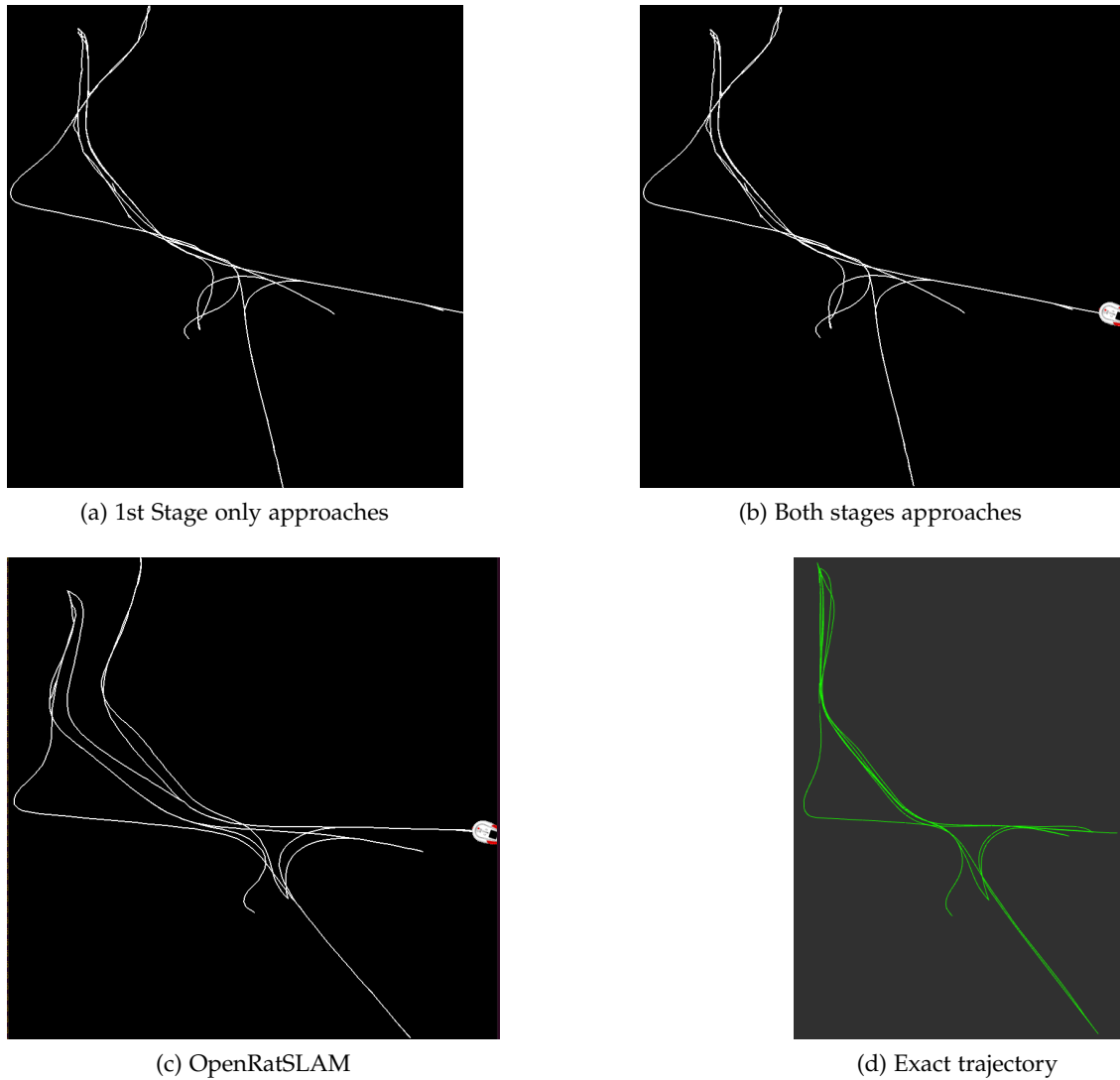
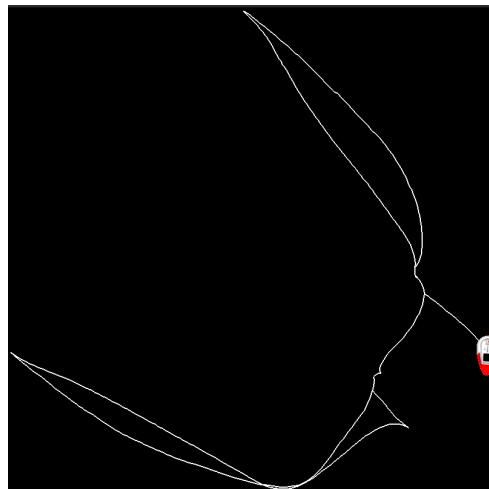
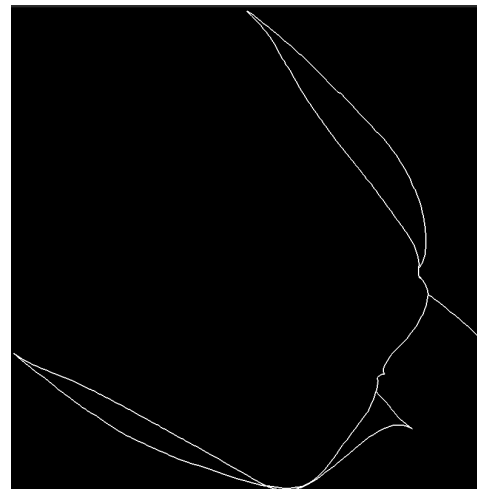


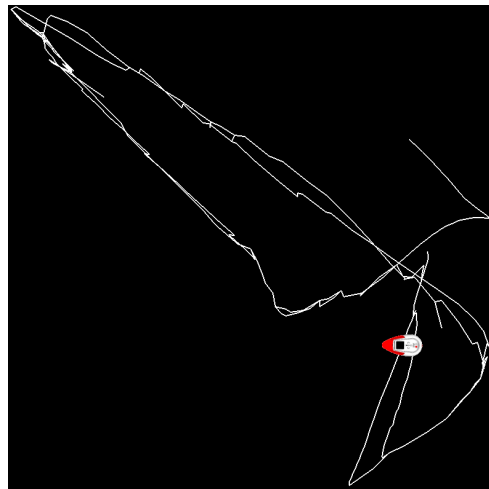
Figure 5.14: Generated experience maps in the house environment



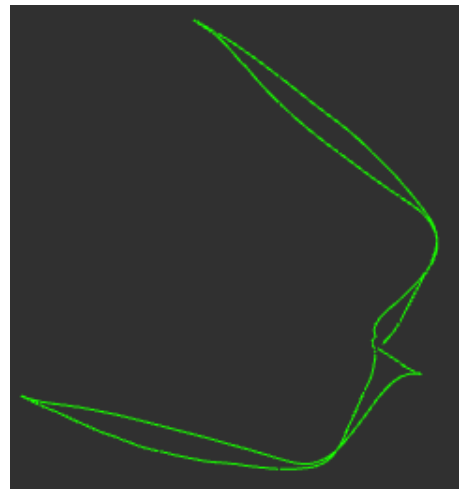
(a) 1st Stage only approaches



(b) Both stages approaches



(c) OpenRatSLAM



(d) Exact trajectory

Figure 5.15: Generated experience maps in the hospital environment

showed almost identical accuracy to the technique with both stages. Furthermore, the first stage-only approach significantly outperformed the both-stage method in terms of consumed memory and slightly in terms of computation time. However, the 2-stage technique proved an ability to eliminate some scenes wrongly classified by the first stage and also showed slightly better accuracy.

Based on these conclusions, the approach with only the first stage is recommended for lower-performance devices, especially in applications with significantly limited memory. This approach usually consumes approximately ten times less memory, and the difference in computation time is also non-negligible. However, if the performance is not the decisive factor, applying the second brings benefits in slightly improved accuracy.

As shown in section 5.8, both approaches proved to be suitable for a local view matching in the RatSLAM algorithm. During the simulation, the process produced stable result trajectories, very similar to the exact ones generated by the simulator.

Both approaches also proved a solid ability to generalization to different environments. For every metric, the results from the environment used for model training and the automatical tuning of parameters were very similar to those from diametrically different environments. In some metrics, the results in the other environments were also better than the results in the warehouse environment used in the development process. This proves that the approach is applicable in almost any indoor environment.

The approaches suggested in this work were also compared to the visual scene recognition used in the OpenRatSLAM approach. The combination of the LiDAR sensor and a camera proved to bring significant benefits compared to the usage of a single camera. The technique using the combination of camera and LiDAR showed significantly better accuracy than the visual scene recognition, especially in a house environment, where the accuracy achieved by suggested approaches was more than twice higher. Furthermore, all the errors produced by methods suggested in this work were close to the threshold, so all the wrongly evaluated matches were still pretty close to each other. On the other hand, the errors produced by the visual scene recognition were considerably larger, sometimes up to 10 times, which very negatively influences the final results produced by RatSLAM.

Memory consumption is another significant advantage of the suggested approaches over visual scene recognition. Not only are templates produced by the first-stage only approach five to six times smaller, but the average number of stored local views is also significantly smaller by both suggested approaches, which brings together huge memory savings, especially in the long run.

The computation time is the only metric in which the visual scene recognition outperformed suggested algorithms. However, because of the sensors' lower frequency and the smaller number of stored local views, thus a lower count of scene recognition executions, the total consumption of the computational resources is still comparable.

According to these results, the addition of a 3D LiDAR sensor showed significantly beneficial. This was proved especially in the hospital environment, see Figure 5.15, where the errors produced by visual scene recognition were so significant that the whole

5 Experiments

SLAM algorithm completely failed, but the approaches suggested in this approach still generated satisfactory results.

6 Conclusion and Future Work

In this thesis, the suitable scene representation and fusion of the data from LiDAR and camera sensors were performed. Afterward, two different approaches for the solution to scene recognition were suggested, and the whole system was integrated with the RatSLAM algorithm. Both proposed techniques operated smoothly during several experiments and significantly outperformed visual scene recognition and OpenRatSLAM.

The addition of a 3D LiDAR sensor to the camera proved beneficial. Not only were the results generated by the proposed methods more precise than those generated by OpenRatSLAM, but they also proved to work in environments where the OpenRatSLAM fails.

6.1 Limitations

Even if the approaches proved good performance in several experiments, there is still a possibility of unknown problems that may occur under several conditions.

Environments

In this thesis, all simulations were performed in static environments. However, in praxis, the environments are rather dynamic and change over time, which might cause problems with scene recognition. Dynamic environments can also contain moving objects, which 3D LiDAR might poorly detect.

Furthermore, the approaches were optimized for indoor environments. In outdoor environments, the ground removal technique might fail because of rugged terrain. Outdoor scenes might also be empty or contain only very far objects, so the DBScan might detect zero clusters which can cause many false negative evaluations.

Sensors

The addition of a LiDAR sensor to the system significantly lowers the sensors' frequency compared to the camera-only configuration. Even if this proved to not be a problem in section 5.8, it could still cause inaccuracies for mobile robots that move with a significantly higher speed than the TurtleBot used for the simulation.

Furthermore, the system was designed and tested with a LiDAR producing relatively sparse point clouds. In the case of usage of some higher quality alternatives, like depth cameras, producing significantly denser point clouds, the system can suffer from

performance issues. However, applying any known downsampling technique before starting the fusion can quickly solve this problem.

6.2 Future Work

The neural system of humans or other mammals is still not wholly inspected and is still a prominent research topic. Therefore, there could come many new discoveries that can serve as an inspiration for the improvement of the RatSLAM or any other biologically inspired SLAM system. For example, the spike cells [61] represent a more accurate model of mammal neural cells and could be effectively used in the RatSLAM's grid network.

Different kinds of neural networks could also be tested for the second stage of the 2-stage approach. For example, HTM [62] proved interesting results in combination with RatSLAM. Furthermore, the PointNet network, used as a feature extractor for the siamese network, can be trained on more suitable datasets. Because of the time constraints and limited offer of publicly available datasets, the network in this work was trained on a dataset containing only single objects instead of whole scenes. Even if this approach proved satisfactory, the more suitable training datasets might also improve the final accuracy of the results.

There are also additional sensors that could further improve the final results in combination with other sensors, like Dynamic Vision Sensors that can improve scene detection with moving objects. The used camera and LiDAR also have a limited field of view. Unlimited scenes could be detected using a panoramic camera and 360° 3D LiDAR. In this case, the scene recognition algorithm could also calculate a relative deviation between two differently rotated locations, which could positively influence the SLAM algorithm. Finally, these additional sensors can also be used to improve the accuracy of the odometry together with the scene recognition.

The color model could also be improved. For example, the Lab sphere can be divided into several sectors. The color would be represented as the id of the sector on the sphere instead of the exact Lab value. Instead of applying the CIE formula, the differences between sectors could be tabulated. This could save computational time and some memory and improve the algorithm's robustness against different light conditions.

List of Figures

2.1	Example of detected features in the image. [16]	7
2.2	Nodes communication structure in the OpenRatSLAM	9
2.3	The OpenRatSLAM system structure. [9]	10
3.1	Visualization of an Lab color representation [43]	17
4.1	Diagram of the ROS nodes in the whole system	20
4.2	Data fusion workflow	24
4.3	Data fusion sensors inputs and generated outputs after each stage	25
4.4	Common scene recognition workflow	29
4.5	An example of the representation of a scene using clustering based approach	29
4.6	Example of the clustered scene after applying the DBScan algorithm	30
4.7	A scheme of the whole local view extraction process	31
4.8	Parametrized sigmoid function	32
4.9	Example of a siamese network used for object comparison	34
4.10	Overview of the two-stage approach	36
5.1	The warehouse world environment 5.1	38
5.2	The small house world environment 5.2	38
5.3	The hospital world environment 5.3	39
5.4	Preview of the animation generated by the analyzer	41
5.5	PR Curves comparing Hierarchical and 2-Stage view matching approaches	42
5.6	Examples of false positives eliminated by the second stage	43
5.7	False positive distances in the warehouse environment	44
5.8	False positive distances in the house environment	45
5.9	False positive distances in the hospital environment	45
5.10	Computation times in the warehouse environment	47
5.11	Computation times in the house environment	48
5.12	Computation times in the hospital environment	49
5.13	Generated experience maps in the warehouse environment	52
5.14	Generated experience maps in the house environment	53
5.15	Generated experience maps in the hospital environment	54

List of Tables

4.1	Relevant topics published by the simulator	21
4.2	Subscribed and published topics by the Data fusion node	21
4.3	Subscribed and published topics by the LV Builder node	22
4.4	Subscribed and published topics by the LV Matching node	22
4.5	Relevant subscribed and published topics by the RatSLAMRos package .	22
4.6	Subscribed topics by the LV Analyzer node	23
4.7	Subscribed topics by the Dataset creator node	23
5.1	Turtlebot3 Waffle PI specification	37
5.2	Accuracy of all approaches in different environments	43
5.3	Average and maximal errors of false positive evaluations in different environments	44
5.4	Average times of LV matching and building in the different environments	48
5.5	Average memory consumption of the algorithms in the different environments	50

Bibliography

- [1] R. T. H. Collis. "Lidar". In: *Appl. Opt.* 9.8 (Aug. 1970), pp. 1782–1788. doi: 10.1364/AO.9.001782. URL: <http://opg.optica.org/ao/abstract.cfm?URI=ao-9-8-1782>.
- [2] T. T. O. Takleh, N. A. Bakar, S. A. Rahman, R. Hamzah, and Z. Aziz. "A brief survey on SLAM methods in autonomous vehicle". In: *International Journal of Engineering & Technology* 7.4 (2018), pp. 38–43.
- [3] T. Taketomi, H. Uchiyama, and S. Ikeda. "Visual SLAM algorithms: A survey from 2010 to 2016". In: *IPSJ Transactions on Computer Vision and Applications* 9.1 (2017), pp. 1–11.
- [4] M. Milford, G. Wyeth, and D. Prasser. "RatSLAM: a hippocampal model for simultaneous localization and mapping". In: *IEEE International Conference on Robotics and Automation, 2004. Proceedings. ICRA '04. 2004*. Vol. 1. 2004, 403–408 Vol.1. doi: 10.1109/ROBOT.2004.1307183.
- [5] D. Ball, S. Heath, J. Wiles, G. Wyeth, P. Corke, and M. Milford. "OpenRatSLAM: an open source brain-based SLAM system". In: *Autonomous Robots* 34.3 (2013), pp. 149–176.
- [6] RatSLAM Ros. URL: <https://github.com/davidmball/ratslam> (visited on 09/09/2022).
- [7] M. J. Milford, J. Wiles, and G. F. Wyeth. "Solving navigational uncertainty using grid cells on robots". In: *PLoS computational biology* 6.11 (2010), e1000995.
- [8] M. J. Milford and G. F. Wyeth. "Mapping a suburb with a single camera using a biologically inspired SLAM system". In: *IEEE Transactions on Robotics* 24.5 (2008), pp. 1038–1053.
- [9] M. Milford and G. Wyeth. "Persistent navigation and mapping using a biologically inspired SLAM system". In: *The International Journal of Robotics Research* 29.9 (2010), pp. 1131–1153.
- [10] M. J. Milford and G. F. Wyeth. "Single camera vision-only SLAM on a suburban road network". In: *2008 IEEE International Conference on Robotics and Automation*. IEEE. 2008, pp. 3684–3689.
- [11] J. O'Keefe. "Place units in the hippocampus of the freely moving rat". In: *Experimental neurology* 51.1 (1976), pp. 78–109.

Bibliography

- [12] E. I. Moser, E. Kropff, M.-B. Moser, et al. "Place cells, grid cells, and the brain's spatial representation system". In: *Annual review of neuroscience* 31.1 (2008), pp. 69–89.
- [13] E. Rosten and T. Drummond. "Machine Learning for High-Speed Corner Detection". In: *Computer Vision – ECCV 2006*. Ed. by A. Leonardis, H. Bischof, and A. Pinz. Berlin, Heidelberg: Springer Berlin Heidelberg, 2006, pp. 430–443. ISBN: 978-3-540-33833-8.
- [14] T. Lindeberg. "Feature Detection with Automatic Scale Selection". English. In: *International Journal of Computer Vision* 30.2 (1998). Cited By :1917, pp. 79–116. url: www.scopus.com.
- [15] S. M. Smith and M. Brady. "SUSAN—A New Approach to Low Level Image Processing". In: *International Journal of Computer Vision* 23 (2004), pp. 45–78.
- [16] *Feature detection and matching with OpenCV*. url: <https://blog.francium.tech/feature - detection - and - matching - with - opencv - 5fd2394a590> (visited on 09/09/2022).
- [17] H. Bay, T. Tuytelaars, and L. Van Gool. "SURF: Speeded Up Robust Features". In: *Computer Vision – ECCV 2006*. Ed. by A. Leonardis, H. Bischof, and A. Pinz. Berlin, Heidelberg: Springer Berlin Heidelberg, 2006, pp. 404–417. ISBN: 978-3-540-33833-8.
- [18] K. Mikolajczyk and C. Schmid. "A Performance Evaluation of Local Descriptors". In: *IEEE transactions on pattern analysis and machine intelligence* 27 (Nov. 2005), pp. 1615–30. doi: 10.1109/TPAMI.2005.188.
- [19] M. Calonder, V. Lepetit, M. Ozuysal, T. Trzcinski, C. Strecha, and P. Fua. "BRIEF: Computing a local binary descriptor very fast". In: *IEEE transactions on pattern analysis and machine intelligence* 34 (Nov. 2011). doi: 10.1109/TPAMI.2011.222.
- [20] J. Philbin, O. Chum, M. Isard, J. Sivic, and A. Zisserman. "Object retrieval with large vocabularies and fast spatial matching". In: *2007 IEEE Conference on Computer Vision and Pattern Recognition*. 2007, pp. 1–8. doi: 10.1109/CVPR.2007.383172.
- [21] Sivic and Zisserman. "Video Google: a text retrieval approach to object matching in videos". In: *Proceedings Ninth IEEE International Conference on Computer Vision*. 2003, 1470–1477 vol.2. doi: 10.1109/ICCV.2003.1238663.
- [22] R. Arandjelović, P. Gronat, A. Torii, T. Pajdla, and J. Sivic. "NetVLAD: CNN architecture for weakly supervised place recognition". In: *IEEE Conference on Computer Vision and Pattern Recognition*. 2016.
- [23] F. Perronnin and C. Dance. "Fisher Kernels on Visual Vocabularies for Image Categorization". In: *2007 IEEE Conference on Computer Vision and Pattern Recognition*. 2007, pp. 1–8. doi: 10.1109/CVPR.2007.383266.
- [24] H. Badino, D. Huber, and T. Kanade. "Real-Time Topometric Localization". In: May 2012, pp. 1635–1642. ISBN: 978-1-4673-1403-9. doi: 10.1109/ICRA.2012.6224716.

- [25] N. Sünderhauf and P. Protzel. "BRIEF-Gist - closing the loop by simple means". In: Sept. 2011, pp. 1234–1241. doi: 10.1109/IROS.2011.6094921.
- [26] B. Zhou, A. Lapedriza, J. Xiao, A. Torralba, and A. Oliva. "Learning Deep Features for Scene Recognition using Places Database". In: *Advances in Neural Information Processing Systems*. Ed. by Z. Ghahramani, M. Welling, C. Cortes, N. Lawrence, and K. Weinberger. Vol. 27. Curran Associates, Inc., 2014. url: [https://proceedings.neurips.cc/paper/2014/file/3fe94a002317b5f9259f82690aeea4cd - Paper.pdf](https://proceedings.neurips.cc/paper/2014/file/3fe94a002317b5f9259f82690aeea4cd-Paper.pdf).
- [27] Y. Yuan, L. Mou, and X. Lu. "Scene Recognition by Manifold Regularized Deep Learning Architecture". In: *IEEE Transactions on Neural Networks and Learning Systems* 26.10 (2015), pp. 2222–2233. doi: 10.1109/TNNLS.2014.2359471.
- [28] P. Fischer, A. Dosovitskiy, and T. Brox. "Descriptor matching with convolutional neural networks: a comparison to sift". In: *arXiv preprint arXiv:1405.5769* (2014).
- [29] A. Krizhevsky, I. Sutskever, and G. Hinton. "Imagenet classification with deep convolutional neural networks". In: Jan. 2012, pp. 1097–1105.
- [30] K. Simonyan and A. Zisserman. "Very Deep Convolutional Networks for Large-Scale Image Recognition". In: *arXiv 1409.1556* (Sept. 2014).
- [31] C. Szegedy, W. Liu, Y. Jia, P. Sermanet, S. Reed, D. Anguelov, D. Erhan, V. Vanhoucke, and A. Rabinovich. "Going deeper with convolutions". In: June 2015, pp. 1–9. doi: 10.1109/CVPR.2015.7298594.
- [32] M. Quigley, K. Conley, B. Gerkey, J. Faust, T. Foote, J. Leibs, R. Wheeler, A. Y. Ng, et al. "ROS: an open-source Robot Operating System". In: *ICRA workshop on open source software*. Vol. 3. 3.2. Kobe, Japan. 2009, p. 5.
- [33] ROS LISP. URL: <https://github.com/ros/roslisp> (visited on 09/09/2022).
- [34] ROS Swift. URL: <https://github.com/tgu/RosSwift> (visited on 09/09/2022).
- [35] G. Bradski and A. Kaehler. "OpenCV". In: *Dr. Dobb's journal of software tools* 3 (2000), p. 120.
- [36] S. Imambi, K. B. Prakash, and G. Kanagachidambaresan. "PyTorch". In: *Programming with TensorFlow*. Springer, 2021, pp. 87–104.
- [37] C. R. Qi, H. Su, K. Mo, and L. J. Guibas. "PointNet: Deep Learning on Point Sets for 3D Classification and Segmentation". In: *arXiv preprint arXiv:1612.00593* (2016).
- [38] PointNet++. URL: <https://github.com/charlesq34/pointnet2> (visited on 09/09/2022).
- [39] Pointnet TensorFlow. URL: <https://github.com/charlesq34/pointnet> (visited on 09/09/2022).
- [40] PointNet PyTorch. URL: <https://github.com/fxia22/pointnet.pytorch> (visited on 09/09/2022).

Bibliography

- [41] C. Connolly and T. Fleiss. "A study of efficiency and accuracy in the transformation from RGB to CIELAB color space". In: *IEEE Transactions on Image Processing* 6.7 (1997), pp. 1046–1048. doi: 10.1109/83.597279.
- [42] N. Proskuriakov, B. Yakovlev, and N. Arkhangelskaia. "Features of the CIE76, CIE-94, and CIE-2000 methods that affect the quality of the determining process of the image average color". In: *Journal of Physics: Conference Series*. Vol. 1791. 1. IOP Publishing. 2021, p. 012107.
- [43] A. Fehir. "Taphonomy's Rainbow: The Introduction and Application of Chromophoric Variance Analysis". PhD thesis. Sept. 2016.
- [44] P. An, T. Ma, K. Yu, B. Fang, J. Zhang, W. Fu, and J. Ma. "Geometric calibration for LiDAR-camera system fusing 3D-2D and 3D-3D point correspondences". In: *Opt. Express* 28.2 (Jan. 2020), pp. 2122–2141. doi: 10.1364/OE.381176. URL: <http://opg.optica.org/oe/abstract.cfm?URI=oe-28-2-2122>.
- [45] A. A. Author, B. B. Author, and C. Author. "Calibration between color camera and 3D LIDAR instruments with a polygonal planar board". In: 10.2 (2005), pp. 49–53.
- [46] R. Hartley and A. Zisserman. *Multiple view geometry in computer vision*. Cambridge university press, 2003.
- [47] M. Himmelsbach, F. V. Hundelshausen, and H.-J. Wuensche. "Fast segmentation of 3D point clouds for ground vehicles". In: *2010 IEEE Intelligent Vehicles Symposium*. IEEE. 2010, pp. 560–565.
- [48] D. Zermas, I. Izzat, and N. Papanikolopoulos. "Fast segmentation of 3d point clouds: A paradigm on lidar data for autonomous vehicle applications". In: *2017 IEEE International Conference on Robotics and Automation (ICRA)*. IEEE. 2017, pp. 5067–5073.
- [49] M. M. Chun and Y. Jiang. "Contextual cueing: Implicit learning and memory of visual context guides spatial attention". In: *Cognitive psychology* 36.1 (1998), pp. 28–71.
- [50] M. Ester, H.-P. Kriegel, J. Sander, X. Xu, et al. "A density-based algorithm for discovering clusters in large spatial databases with noise." In: *kdd*. Vol. 96. 34. 1996, pp. 226–231.
- [51] C. B. Barber, D. P. Dobkin, and H. Huhdanpaa. "The quickhull algorithm for convex hulls". In: *ACM Transactions on Mathematical Software (TOMS)* 22.4 (1996), pp. 469–483.
- [52] M. Mitchell. *An introduction to genetic algorithms*. MIT press, 1998.
- [53] X. Shen, C. Wang, C. Wen, W. Liu, X. Sun, and J. Li. "Discriminative learning of point cloud feature descriptors based on siamese network". In: *IGARSS 2018-2018 IEEE International Geoscience and Remote Sensing Symposium*. IEEE. 2018, pp. 4519–4522.

- [54] Z. Wu, S. Song, A. Khosla, F. Yu, L. Zhang, X. Tang, and J. Xiao. “3d shapenets: A deep representation for volumetric shapes”. In: *Proceedings of the IEEE conference on computer vision and pattern recognition*. 2015, pp. 1912–1920.
- [55] Y. LeCun, D. Touresky, G. Hinton, and T. Sejnowski. “A theoretical framework for back-propagation”. In: *Proceedings of the 1988 connectionist models summer school*. Vol. 1. 1988, pp. 21–28.
- [56] W. James and C. Stein. “Estimation with quadratic loss”. In: *Breakthroughs in statistics*. Springer, 1992, pp. 443–460.
- [57] *Velodyne Simulator*. URL: https://github.com/lmark1/velodyne_simulator (visited on 09/06/2022).
- [58] *Warehouse simulation toolkit*. URL: https://github.com/wh200720041/warehouse_simulation_toolkit (visited on 09/06/2022).
- [59] *AWS Robomaker Small House World*. URL: <https://github.com/aws-robotics/aws-robomaker-small-house-world> (visited on 09/06/2022).
- [60] *AWS Robomaker Hospital World*. URL: <https://github.com/aws-robotics/aws-robomaker-hospital-world> (visited on 09/06/2022).
- [61] S. Kim, S. Park, B. Na, and S. Yoon. “Spiking-yolo: spiking neural network for energy-efficient object detection”. In: *Proceedings of the AAAI conference on artificial intelligence*. Vol. 34. 07. 2020, pp. 11270–11277.
- [62] S. Schubert, P. Neubert, and P. Protzel. “Towards combining a neocortex model with entorhinal grid cells for mobile robot localization”. In: *2019 European Conference on Mobile Robots (ECMR)*. 2019, pp. 1–8. doi: 10.1109/ECMR.2019.8870939.